Scale-dependent controls on forest carbon uptake across hydroclimatic extremes

Laura Rez[1], Timo Vesala[2,3], Eli Tziperman[4], Pasi Kolari[2], Eyal Rotenberg[1], Rachamim Rubin[1], and Dan Yakir[1]

[1]Department of Earth and Planetary Sciences, The Weizmann Institute of Science, Rehovot, Israel

[2]Institute of Atmospheric and Earth System Research/Physics, Faculty of Science, University of Helsinki, Finland

[3]Institute of Atmospheric and Earth System Research/Forest Sciences, Faculty of Agriculture and Forestry, University of Helsinki, Finland

[4]Department of Earth and Planetary Sciences and School of Engineering and Applied Sciences, Harvard University, Cambridge, MA, USA

Authors for correspondence:

Dan Yakir

Email: dan.yakir@weizmann.ac.il

Keywords - 6-10

Carbon storage, controlling factors, machine learning, SHAP

Peer review status

This paper is a non-peer reviewed preprint submitted to EarthArXiv. The article is currently under review by One Earth.

Abstract

Conifer forests span some of the most climatically contrasting environments on Earth, from energy-limited Boreal systems to water-limited semi-arid ecosystems. Whether their carbon uptake is governed by universal drivers or by site-specific boundary conditions remains unresolved. Using more than two decades of eddy-covariance and multi-depth soil moisture measurements from two climatic end-members of evergreen needleleaf forests, Hyytiälä, Finland (Boreal) and Yatir, Israel (semi-arid Mediterranean), we isolate the ecophysiological controls on carbon uptake by restricting the analysis to photosynthetically active radiation (PAR)-saturated conditions and explicitly separating seasonal dynamics from daily residual variability. For each dataset, we apply Random Forest modelling (tested against baseline Generalized Linear & Additive Models) with SHAP analysis to identify dominant drivers and environmental thresholds.

At the seasonal scale, NEP was governed by distinct boundary conditions in each forest. In Hyytiälä, precipitation had dominant control, sustaining evapotranspiration and reflecting a radiation regime characterized by high diffuse fractions. In Yatir, deep soil water availability controlled both the timing and magnitude of productivity, with a critical threshold at ∼15.9 %vol in the deepest measured layer (∼45 cm). This threshold marked the transition from dry-season legacy constraints, where vertical soil potential gradients limit root uptake, to conditions permitting sustained transpiration and productivity.

At the daily residual scale, both forests showed strong sensitivity to shortwave radiation and vapour pressure deficit (VPD), despite contrasting climatologies. Elevated VPD reduced peak daily productivity by more than 50% at both sites, although sufficient deep soil moisture mitigated this effect in the semi-arid forest. Notably, both forests exhibited a similar optimal air temperature range (14–20 °C), indicating a conserved physiological optimum despite divergent hydroclimatic limitations.

Our results demonstrate that carbon uptake in evergreen needleleaf forests is structured by site-specific hydrological boundary conditions at seasonal scales, while atmospheric stress regulates short-term variability. This scale-dependent hierarchy of controls challenges the notion of universal productivity drivers and highlights the importance of subsurface hydrology and rainfall regime characteristics for predicting forest carbon responses to climate change.

1 Introduction

Forest ecosystems play an important role in the global carbon cycle and in mediating climate change, capturing 3.5-3.6 Pg C yr^{-1} fossil fuel emissions and storing an estimated 870 Pg of carbon in biomass and soil (Pan et al., 2024; IPCC, 2023). Over recent decades, the global forest

carbon sink has remained relatively stable despite trend changes in global atmospheric CO_2 and temperature – this apparent stability, however, masks substantial regional variability, with sink strength changing by more than 30% across regions (Pan et al., 2024; Hubau et al., 2020). In addition to anthropogenic forest thinning and planting, global warming significantly changes sink strength by influencing ecosystem respiration, enabling pest outbreaks and wildfires, and increasing sensitivity to climate extremes (Settele et al., 2014; IPCC, 2023; Curtis and Gough, 2018; Park et al., 2019; Hammond et al., 2022). The latter poses a sustained threat to productivity, the crux of input to the forest carbon balance and carbon-sink activity.

Studies have demonstrated that factors such as leaf-area index, shortwave radiation, precipitation, air temperature, and vapour-pressure deficit (VPD) control productivity globally and across biomes (Estiarte et al., 2016; Kong et al., 2022; Zhou et al., 2023; Shi et al., 2023). There is evidence, however, that responses to climate drivers and stress is highly regional due to unique site characteristics, including stand age and management, unequal (regional) intensification of climate extremes, and offsets between the hydrologic and productive seasons (Pregitzer and Euskirchen, 2004; Thom et al., 2019; Park et al., 2019; Bartsch et al., 2020; Li et al., 2022; Markos et al., 2024). In addition, forest productivity is potentially undergoing concurrent long-term changes driven by rising atmospheric CO_2, climate warming, and alterations in stand age, structure, and management practices (Pascual et al., 2026). The effects of these, however, has been inconsistent within plant-functional type and across stand age (Hubau et al., 2020; Van Der Sleen et al., 2015; Hättenschwiler et al., 1997). Therefore, while photosynthesis may respond similarly across ecosystems to main climate drivers, there are likely site-specific limitations and conditions that influence how productive a given site may be, and how precisely we can explain and model these changes. The key question remains - are there universal environmental drivers that regulate forest productivity, or do site-specific boundary conditions govern carbon uptake in different climatic contexts? Moreover, how can we quantitatively compare the two effects?

Evergreen needle-forests (ENF) are a useful baseline ecosystem for evaluating this question, given that they are important global carbon sinks that span a broad range of biomes (Pastorello et al., 2020). To this point, ENFs have adapted to contrasting climates such as the cold-wet Boreal and the hot-dry Mediterranean, which are both regions that are currently potentially at risk of becoming carbon sources due to unique combinations of drought, rising temperatures and human interference (Appiagyei et al., 2022; Zhang et al., 2009; Beer et al., 2010; IPCC, 2023). The sensitivity in eco-physiological response to climate and environmental drivers in these contrasting environments would therefore reveal whether there is a consistent response across regions, or region-based boundary conditions.

Despite persistent efforts to determine the controlling factors on forest productivity worldwide, not much emphasis has been put on isolating productivity within its temporal boundaries. Productivity has been assessed- either gross primary production (GPP) or net ecosystem

production (NEP, GPP factoring in ecosystem respiration), from sub-daily to annual scales (Zhou et al., 2023; Ezhova et al., 2025; Sun et al., 2018; Wang et al., 2022) while including seasons or times of the day when forests, especially in the northern hemisphere, are inactive or are responding to changing light conditions (i.e., winter, dry-season, sunrise/sunset). At the annual scale, this may lead to an oversimplification of the effect of temperature and precipitation due to a strong seasonal cycle that masks daily variability and weather event intensification under climate change (Smith, 2011).

At the daily and sub-daily scale, photosynthesis exhibits a strong, at least partly trivial response to changes in light intensity associated with diurnal and seasonal light cycles. The strong response in GPP and NEP to light at these scales comes from the linear portion of the light response curve (Marshall and Biscoe, 1980), which correlates strongly with the solar angle and light intensity changing in the early and later hours of the day. As a result, shortwave radiation or photosynthetically-active radiation (PAR, which is strongly correlated with the former) often emerge as dominant controlling factors over GPP and NEP (Mäkelä et al., 2006; Wu et al., 2017; Han et al., 2020; Zhou et al., 2023), potentially masking or down-playing the importance of other atmospheric or environmental factors.

While these approaches have yielded valuable insights, they are commonly limited by (1) short observational records that face challenges in separating natural variability from discrete responses to weather extremes and long-term trends, (2) aggregation across seasonal and diurnal cycles, and (3) an emphasis on correlation rather than quantification of control. These limitations are further compounded by the scarcity of long-term study sites with multi-depth soil moisture measurements (Pastorello et al., 2020), restricting the ability to assess the role of subsurface hydrology in regulating productivity.

Here, we introduce a framework to disentangle the controls on forest carbon uptake across timescales. Specifically, we (1) restrict analysis to PAR-saturated conditions to remove the trivial light-driven response, (2) decompose NEP into seasonal and residual components to isolate slow versus fast dynamics, and (3) apply explainable machine learning to quantify scale-dependent controls and thresholds. This approach allows us to test whether environmental drivers are consistent across timescales or reorganize under different boundary conditions. In this context, we focus on variables that directly constrain ecosystem function at seasonal to daily timescales, rather than slower-changing background drivers such as atmospheric CO_2 concentration.

2 Materials and methods

2.1 Locations

This study aims to compare the controlling factors for carbon capture in two evergreen-needle forests (ENFs), each containing long-term eddy-covariance FLUXNET towers, on opposite ends of the conifer distribution range: the Boreal Hyytiälä forest, Finland (61°51'N,24°17'E, 160-180 m a.s.l., SMEAR II site record 1997-current - "HYY" (Hari et al., 1994)) and the semi-arid Mediterranean Yatir forest, Israel (31°20'N,35°3'E, 550-700 m a.s.l., site record 2000-current - "YAT" (Rotenberg and Yakir, 2010)). Both forests were planted primarily with pine species in the 1960's: Aleppo pine (*Pinus halepensis*) in YAT at the desert edge, and Scots pine (*Pinus sylvestris* L.) in HYY, after a prescribed burning in 1962 (Aslan et al., 2024). Both forests also share a similar, relatively shallow soil-profile that is on average less than one metre (Food and Agriculture Organization of the United Nations and UNESCO, 1990).

HYY is the northernmost ENF site with minimum 20-year record (including soil-water content at multiple depths) and a mean annual temperature (MAT) that is above zero (3.8 °C, Suni et al. (2003); Pastorello et al. (2020)). There, the forest receives a mean annual precipitation (MAP) of 709 mm, and the productive season is constrained by temperature (mean daily temperature range of approximately -20 °C to 23 °C) and light sensitivity (Suni et al., 2003; Tanja et al., 2003). Yatir is the southernmost ENF site in the northern hemisphere, and there the productive season is less limited by temperature (MAT range of 4 °C to 32 °C), and mainly by a short and modest rainfall season (285 mm within October-April). Given the respective temperature and rainfall limitations, both forests experience an approximate six-month inactive (non-productive) season - the winter dormancy in HYY (November-April), and the hot summer dry-season in YAT (May-October).

2.2 Data

25-year records from both sites contain the following common measurements: Shortwave radiation (SW), longwave radiation (LW), air temperature (TA), relative humidity (RH), vapor-pressure-deficit (VPD), air pressure (PA), precipitation (P), wind-speed (WS), soil water content (SWC) at three approximate depths (0-15;25-35;≥45 cm; referred to as I,II,III), and net ecosystem production (NEP, the inverse sign of the measured net ecosystem exchange of CO_2). Note that positive NEP indicates carbon uptake by the ecosystem, while negative NEP indicates carbon lost to the atmosphere, and that in this study, we are presenting values of NEP in grams of Carbon.

We kept VPD and dropped RH from the feature (variable) list. While VPD is calculated from TA and RH, and is therefore correlated with both, TA and VPD have unique implications on leaf biochemical and stomatal responses (respectively), whereas RH would neither significantly improve

model-learning nor interpretation of the results. Half-hourly data was aggregated to daily using the sum for P and NEP, and the mean for the remaining features. Due to constraints in the SWC records in both locations, the portion of data used for modelling was refined to approx. 20 years for both sites: in HYY, 1998-2017; and YAT, 2005-2025, while shorter records of evapotranspiration (ET), diffuse shortwave radiation (SW_{DIF}) and soil temperature (TS) were kept to analyze results. Table 1 summarizes the acronyms, variable units and record lengths (where applicable) used in this study.

Table 1: List of common acronyms throughout the study, with units and approximate record length of measurements and derived values (the shortest record length given the two forests).

Acronym	Term	Description
HYY	Hyytiälä forest, Finland	Boreal
YAT	Yatir forest, Israel	Semi-arid
S	"Seasonal"	Referring to the seasonal dataset, 2.2.2
R	"Residual"	Referring to residual dataset, 2.2.2
ET	Evapotranspiration	$\mathrm{mm\,day^{-1}}$, $\sim$ 25 years
LW	Direct longwave radiation	$\mathrm{W\,m^{-2}}$, $\sim$ 25 years
NEP	Net ecosystem production	$\mathrm{g\text{-}C\ m^{-2}\,day^{-1}}$, $\sim$ 25 years
P	Precipitation	$\mathrm{mm\,day^{-1}}$, $\sim$ 25 years
PA	Air pressure	Pa, $\sim$ 25 years
PAR	Photosynthetically active radiation	$\mathrm{\mu mol\,m^{-2}\,s^{-1}}$, $\sim$ 10 years
RH	Relative humidity	%, $\sim$ 25 years
SW	Direct shortwave radiation	$\mathrm{W\,m^{-2}}$, $\sim$ 25 years
SW_{DIF}	Diffuse shortwave radiation	$\mathrm{W\,m^{-2}}$, $\sim$ 10 years
SWC	Soil water content	%vol, $\sim$ 20 years
SWP	Soil water potential	MPa, $\sim$ 20 years
TA	Air temperature	°C, $\sim$ 25 years
TS	YAT soil temperature	°C, TS_{II}:$\sim$ 15 years; TS_{III}:$\sim$ 5 years
VPD	Vapour-pressure deficit	hPa, $\sim$ 25 years
WS	Wind speed	$\mathrm{m\,s^{-1}}$, $\sim$ 25 years

2.2.1 Trimming dataset for productivity

To focus on the non-trivial ecophysiological responses, we removed the linear light-limited portion of the photosynthetic response curve (Marshall and Biscoe, 1980), and focused on the remaining saturated portion. In ENF trees, these two parts of the curve are consistently separated by a boundary of approximately 500 $\mathrm{\mu mol\,m^{-2}\,s^{-1}}$ PAR, as is seen in Figure 1 for HYY and YAT, and

other ENF studies (Leverenz, 1987; Cernusak and Marshall, 2000; Remke et al., 2020). Using the coordinates for each forest and a solar zenith angle filter of $\leq$ 70 degrees, which correlates to a PAR value of $\geq$ 500 µmol m^{-2} s^{-1}, we filtered respective half-hourly data from each forest and effectively eliminated the expected linear portion from the remainder of the light response curve. We used pvlib Location and get-solarposition tools for this calculation (Anderson et al., 2023).

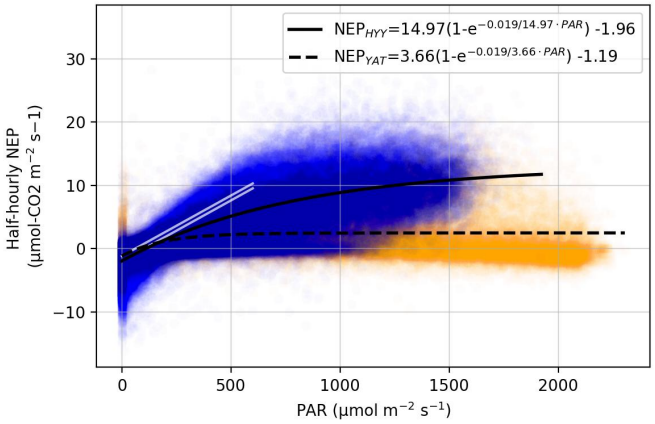

Figure 1: Light response curves for HYY (blue, solid) and YAT (yellow, dashed) alongside the linear projection of the peak efficiency (white lines) in low light conditions

.

2.2.2 Obtaining residual (R) data

To separate slow seasonal controls from short-term variability, we decomposed all variables into seasonal and residual components. The independent variables and NEP in each forest contain strong seasonal signals with either an annual or 6-month dominant period (365.25 and 183 days, respectively, obtained by Fourier transform), which tend to dominate the fitting and learning process when modelling NEP. To study the controlling factors on a daily timescale, it was necessary to produce a dataset where the effect from seasonality had been removed, and only the residual variability effect remained. For each forest, first, the historical daily mean and standard deviation for each variable, including NEP, was calculated from a rolling mean of window size 9 days x 20 years, centred on the day of year, thus creating the seasonal dataset. The seasonal values were then subtracted from the respective original variable's data, creating the residual (R) dataset (see bottom left in Figure 2 for visualization). The seasonal and residual datasets are used to train separate models, leading to separate SHAP analyses for each dataset (see orange and blue tracks in Figure 2), explained further in 2.4.

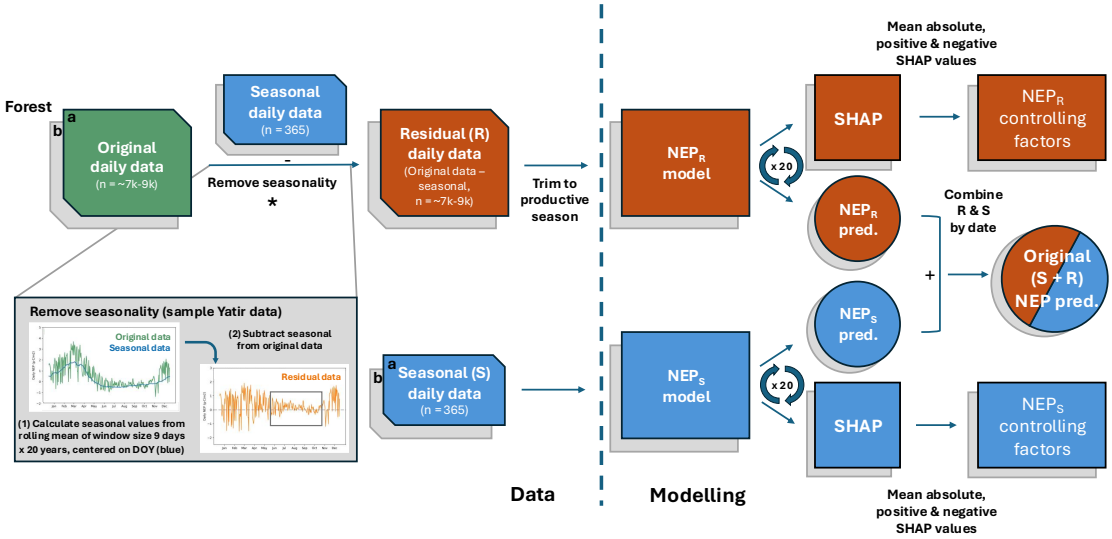

Figure 2: General scheme for the data pre-processing and model flow with SHAP, for two forests (a, b). A key data pre-processing step, the removal of seasonality to isolate residual variances, is illustrated on the left with sample NEP data from YAT. In the modelling side, input data (residual (R) and seasonal (S), following parallel tracks) is received by a given model (GLM, GAM, or RF), which is trained over 20 random iterations leading to 20 trained models per model type and dataset (R or S). We use the 20 trained models to obtain mean NEP_R and NEP_S predictions, and respective SHAP analysis outputs. This step is repeated for each model type, and the overall scheme is repeated for each forest (HYY and YAT).

2.2.3 Studying the productive season

Both forests are located in the northern-hemisphere and experience similar seasonality in solar radiation. The productive season in HYY, however, is constrained by temperature due to the below-zero winters, while the productive season in YAT is limited by a hot summer dry-season. We calculated the start and end of the productive season for each forest using these environmental boundary conditions, while further incorporating, for modelling purposes, that the productive season is described by high variance as opposed to the dormant season when residual NEP response nearly flat-lines (see box over residual data in Figure 2, and section **??** in Supplementary Materials for full productive season start- and end-day calculation). This was necessary, because the flat-line dormant response is a separate phenomenon that would only confuse the models from learning structure related to actively changing biological and ecophysiological responses. The more accurately-defined yearly start and end day-of-year of the productive season captured more relevant data for the models to learn from.

2.3 Baseline models and Random Forest

We tested Random Forest Modelling (RF, RandomForestRegressor from Scikit-learn (Pedregosa et al., 2011)) against baseline Generalized Linear Model (GLM) and Generalized Additive Model (GAM) from statsmodels (Seabold and Perktold, 2010). While the GLM is simple to interpret and the GAM can capture non-linear relationships, the RF architecture, which is based on conditional logic, additionally learns interactions between features, which we expect to be key in modelling NEP_R, the datasets with the most complexity. The data was split 90-10 for train-test sets for all models, while hyper-parameter optimization for RF and GAM were performed separately on an 80-20 split. Model hyper-parameters can be found in Supplementary Materials, Table **??**. Data splitting and model fitting were repeated for 20 random seeds, and the predictions and SHAP values are averages from these runs. An XGBoost model was also tested, however the model was prone to over-fitting and eventually performed similarly to RF when minimizing hyper-parameters that led to this overfit, so it is not presented.

2.4 SHAP analysis

SHAP (Shapley additive explanations) analysis has become a complementary tool in classical machine learning (ML) that is used to quantify the probability of feature importance in a model; i.e., quantify a variable's contribution to the model's predicted outcome. Built upon multiple-player Game Theory (Von Neumann and Morgenstern, 2007), Shapley values (SHAP values) have a unique robustness originating from the model's formulation that adheres to certain crucial mathematical and modelling properties (additivity, local accuracy, missingness, and consistency) (Lundberg, 2017). In a regression analysis, a SHAP value of a respective variable is a probabilistic quantification of that variables contribution, *in relative units*, to the predicted value. The SHAP value (Φ) for a given variable, i, for a single instance of data, is given by:

$$\Phi_i = \sum_{S \subseteq \{1,\ldots,p\}\{i\}} \frac{|S|!(p-|S|-1)!}{p!}[val(S \cup \{i\}) - val(S)]$$

The first term in the sum calculates the probability from grouping variable i within a grouping, S, of all other independent variables (p). The marginal contribution of variable i is calculated in the second term of the sum, using a value function (val) - which, for instance, can be a trained RF model (respective to each physical forest). The marginal contribution is the output of the model when grouping S includes variable i, subtracted by the prediction when variable i is excluded. We used the SHAP Python package Lundberg (2017) with standard interventional SHAP to evaluate the contribution of all variables, handling separately any potentially correlated variables.

We applied SHAP analysis to each trained model (Fig.2), resulting in mean SHAP values

from the 20 random seed runs. To determine the controlling factors in a given dataset (seasonal or residual, HYY or YAT), we calculated the respective percent contribution of a variable i (C_i) using the mean absolute SHAP values (Φ) of all variables (P) across the 20 random runs. The mean absolute SHAP value of a variable i is calculated from all instances t in the dataset:

$$\Phi_i = mean[\sum_t |\Phi_i|]$$

$$C_i = \frac{\Phi_i}{\sum_P \Phi} * 100$$

3 Results

Using a scale-dependent framework, we evaluated controls on seasonal NEP, followed by residual (daily anomaly) variability. First, we characterized the PAR-saturated, scale-dependent datasets, and tested the quality of multiple model predictions. Next, we applied SHAP analysis to quantify the controlling factors at each timescale, and, using these values, derived environmental and climatic thresholds over NEP in each forest.

3.1 Input data characteristics

3.1.1 Productive season

In HYY, the productive season ranged from April 11th (±12 days) to October 26th (±11 days) consistent with Mäkelä et al. (2006); Böttcher et al. (2014), lasting a mean 198 days; in YAT, the season spanned from December 4th (±21 days) to May 28th (±7 days), lasting ∼175 days (all dates in Table **??**). Under PAR-saturated conditions, HYY received more hours of radiation than YAT (1767 vs 1430 h, $p<10^{-9}$), whereas YAT received a greater total shortwave energy input (2.97 vs 2.68 GJ m^{-2}, $p<10^{-5}$) (Table **??**). Overall, under PAR-saturated conditions, the productive season in HYY was limited by the intensity of incoming SW radiation, while the season in YAT was limited by the total hours of radiation.

3.1.2 Descriptive statistics

The original datasets contained strong seasonal correlations among radiation, temperature, VPD, and soil moisture, which were largely absent in the residual datasets (see seasonal trends in Fig.3 and correlation matrices in A1). Hierarchal clustering revealed two main groups, consistent in each forest and dataset: radiation-related variables (SW, TA, VPD), and precipitation-related variables

(P, PA, RH, SWC, WS) (see groups 1 and 2 in Fig. A1). NEP was grouped in the radiation cluster in HYY and in the precipitation cluster in YAT.

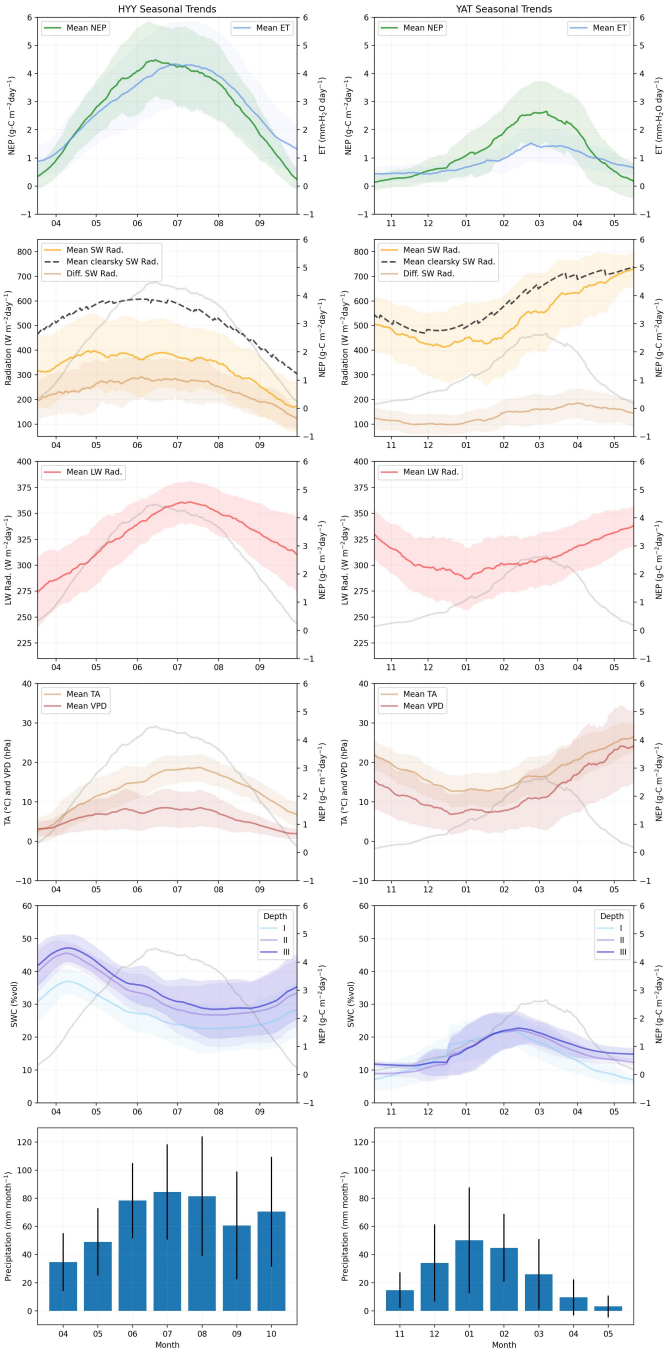

Figure 3: Seasonal trends in NEP, ET and all features in HYY (left) and YAT (right). NEP_S and ET_S are strongly correlated in both forests ($R \geq 0.97$), but diverge in closest feature correlation: VPD in HYY ($R=0.97$) and SWC ($R \geq 0.86$) in YAT; see correlation matrices in A1. Recall that seasonal values were obtained from a rolling window of size nine days by 20 years, and therefore, any direct daily response between NEP and a feature has been smoothed over. The values presented here represent only a general seasonal cycle.

3.2 RF, GAM, and GLM model performance: accuracy and reliability

3.2.1 Model accuracy in predicting NEP_S and NEP_R

NEP_S was well-predicted across all models ($R^2_{test} > 0.94$), whereas model performance varied in predicting NEP_R (Fig.A2-A3). RF outperformed GLM and GAM (R^2_{test} ≈0.67 vs. 0.46-0.64), though there was a systematic underestimation of extreme residual values in all models (90th percentile absolute NEP_R in HYY underestimated by 26%, 34% and 51%, and in YAT by 30%, 41%, and 54%, for RF, GAM, and GLM, respectively).

We analyzed the top ten instances of high and low NEP_R in HYY and YAT and found that extreme NEP_R was underestimated in rare cases of compounding VPD, TA and SWC conditions, and by confounding rainfall and SW inputs. For example, peak NEP_R in YAT was a result of seasonally high SWC_R III and low VPD_R in April, which occurred in ∼7% of the dataset, while peak NEP_R in HYY was associated with an optimal combination of VPD_R, TA_R and SWC_R in June and July, which totalled 3.1% of instances. A full description of the cases that lead to model underestimation is given in Supplementary Materials **??**.

3.2.2 RF learns extreme values without over-fitting

RF, GAM and GLM have inherent structural and methodological differences in learning and fitting to data which affect the reliability of their predictions. We found that the GLM and GAM underestimated peak NEP_R due to a modelling reliance on perpetually non-normally distributed residuals (statistical term, not the residual dataset), and extrapolation of extreme values. In contrast, RF learned variance in NEP_R better, especially negative NEP_R, without over-fitting as confirmed by permutation tests (A4). Based on its superior performance and more robust outputs, the RF models were used in all subsequent SHAP analyses.

3.3 Seasonal NEP (NEP_S) controlling factors in HYY and YAT

The driving factors for NEP_S in HYY were P_S and VPD_S (48.8% and 29.4%, respectively), whereas in YAT SWC_S dominated (79.6%), with the deepest layer contributing more than half of the control (Fig.4.a&e). All seasonal controlling factors were found to have a mean negative influence on NEP_S (blue arrows in Fig.4). In HYY, this was due to a shorter but more profound negative effect of low P_S amounts in the beginning and end of the productive season, relative to the positive effect of P_S during the peak productive months (Fig.4.b). In YAT, the strong positive effect of SWC III during the wet season was outweighed by the relatively moderate negative-effect during the dry season, but which persisted over a longer period of time (Fig.4.f). Based on the apparent seasonal transitions from negative to positive SHAP values for key controlling factors in HYY and

YAT in Figure 4b&f, respectively, we were able to calculate certain corresponding environmental thresholds from the original seasonal data that is presented next in 3.4.

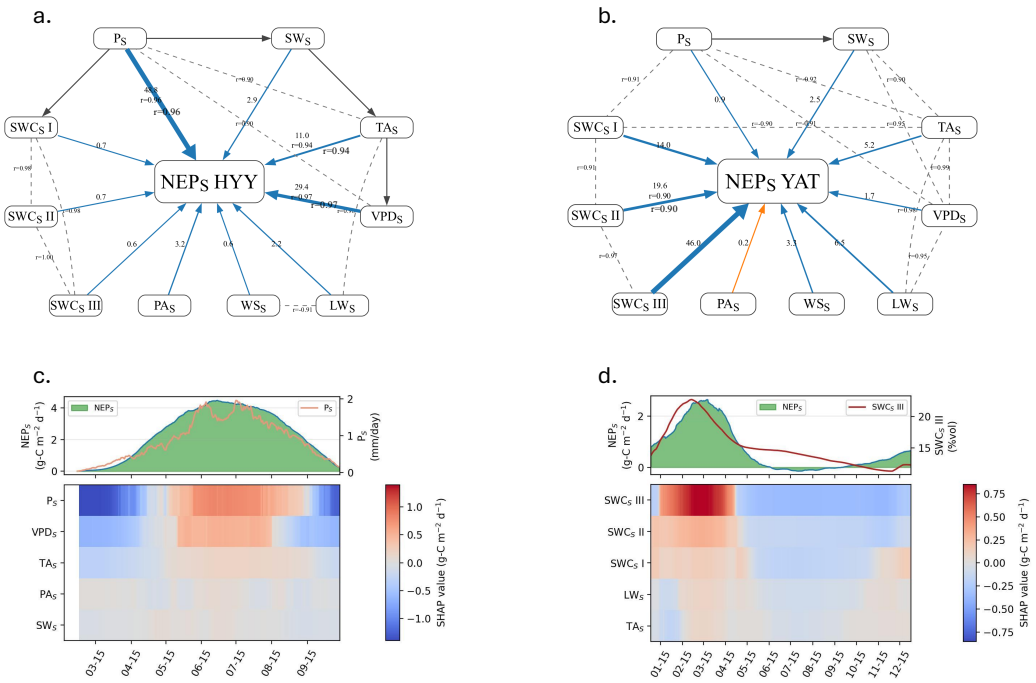

Figure 4: Controlling factors (CF) for NEP_S obtained from SHAP analysis for HYY (left) and YAT (right). All factors are shown in (a,b), where arrow thickness and values represent the magnitude of a feature's control as % within a given model (for calculation see 2.4), and the colour gives the mean sign of influence (positive=orange, negative=blue). Correlations above R=0.9 are given by the dashed lines, and solid black arrows represent known direct influences between variables where a strong correlation was not present. Seasonal daily SHAP values for the top five controlling factors in HYY and YAT are given in (c, d), respectively, highlighting the mean changes from negative to positive influence (blue to red) over the productive season in each forest.

3.4 Climatic and environmental thresholds derived from SHAP values

In HYY, TA_S and VPD_S became positive influences on NEP_S when greater than 11.2 ±0.26 °C (Fig.5c1) and 6.2 ±0.16 hPa (Fig.5b1), respectively, with a peak positive influence from TA_S within 14.8-18.7 °C (see dashed lines in Fig.5 subplots). Since rainfall is highly variable and a threshold for mean daily seasonal rainfall is ambiguous, we focused instead on the behaviour of the curve and found that P_S reached a saturated influence on NEP_S during its peak in June and July (Fig.5a1).

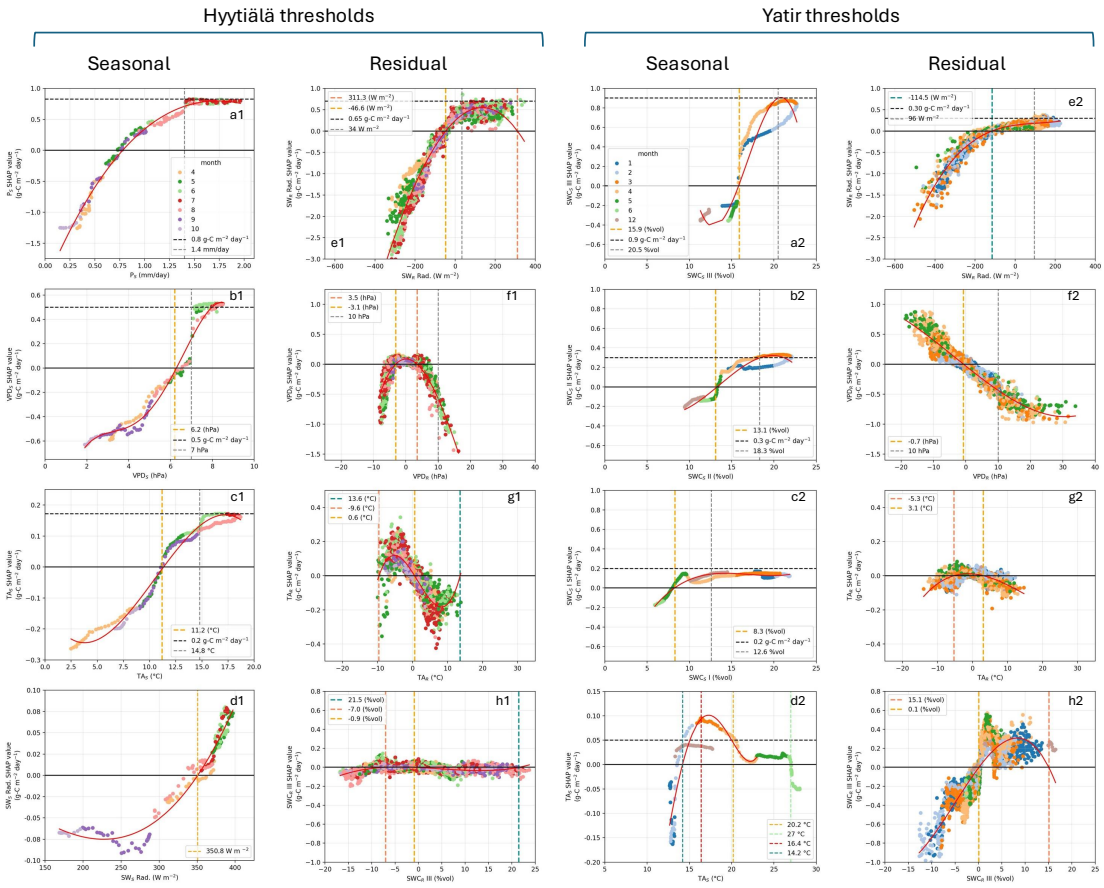

Figure 5: Climatic and environmental thresholds for the main controlling factors of seasonal (S) and residual (R) NEP in HYY (left) and YAT (right). The thresholds are obtained from a best-fit polynomial function (red curve) between the respective dataset's SHAP values and a given controlling feature, particularly (1) where the SHAP values cross y=0 and shift from a negative to a positive influence on NEP and carbon uptake, or vice-versa (see dashed yellow, orange and/or teal vertical lines); and (2) where SHAP values saturate, and the associated feature ultimately begins to have a saturated influence on NEP (see grey and black dashed lines for the respective feature and SHAP value when saturation effect begins).

In YAT, sharp hysteresis curves for SWC_S II & III (Fig.5a2,b2) exposed thresholds of 13.1 ±0.07 %vol & 15.9 ± 0.08 %vol, respectively, while SWC I became a positive influence on NEP_S when greater than 8.3 ±0.20 %vol. The hysteresis curves also revealed a lower positive influence from SWC_S II & III on NEP_S in January-February compared to March-April, for a similar range of SWC_S (approx. 16-23 %vol). Finally, in YAT, TA_S positively influenced NEP_S when ranging between 14-27 °C, with a peak positive effect at 16.4 °C which is within the same peak TA_S range as HYY.

3.5 Residual NEP (NEP_R) controlling factors

Similar to Figure 4, controlling factors for NEP_R are given in Figure 6a,b, and the daily SHAP value heatmaps from a sample productive season are given in c,d, along with related time-series of the original residual data. In both forests, NEP_R was controlled by shortwave radiation (51% in HYY; 21% in YAT), with additional contributions from VPD and deep soil moisture in YAT (Fig. 5a,b).

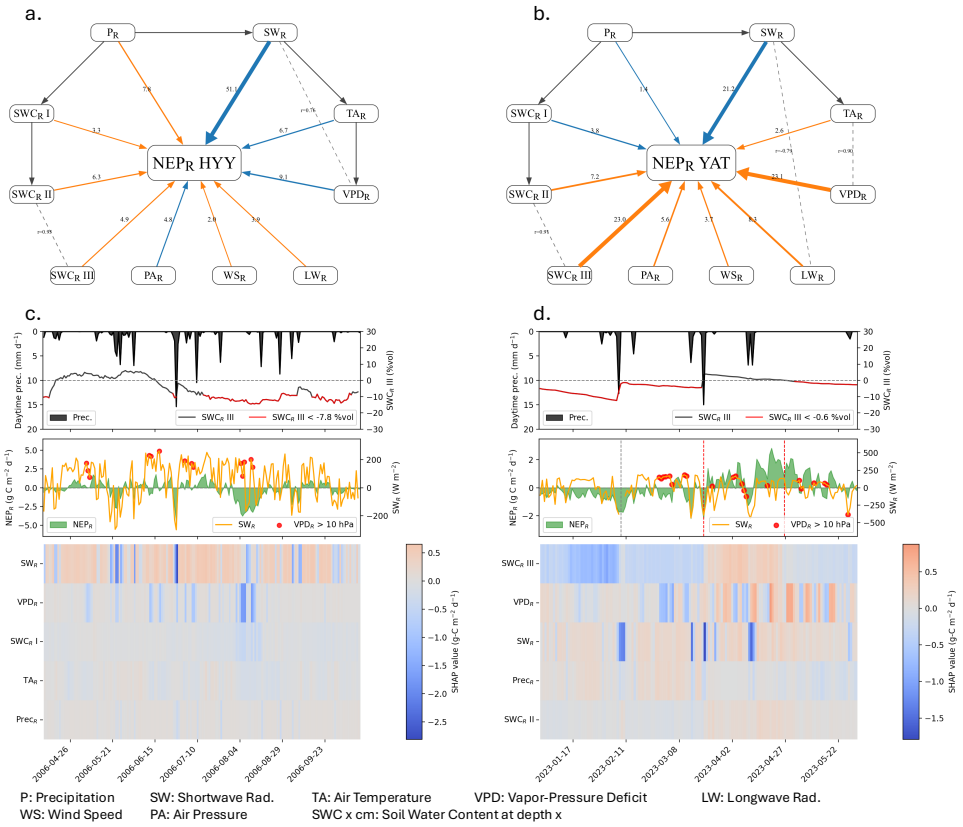

Figure 6: Same as Figure 4, but for residual (R) NEP. In (a,b), we see a mixed contribution in each forest from SW_R, VPD_R, and SWC_R. Subplots (c, d) give sample productive seasons 2006 and 2022-2023 for HYY and YAT, respectively, to help visualize the daily influence on NEP_R (green), revealing a common residual drop in productivity from daytime rainfall events (black, top) that influence SW_R (yellow, drops to negative and has negative/blue SHAP value). In other instances, excessively high VPD_R greater than seasonal values by 10 hPa (red markers, negative SHAP influence) also results in negative NEP_R, except in YAT, when SWC_R III is above the seasonal threshold (see upper panels; SWC_R II and III is highlighted in red in HYY and YAT, respectively, when values drop below the thresholds determined in section 3.4.

3.5.1 High sensitivity to VPD_R

VPD_R exerted a clear negative control in both forests when values rose above ∼1 hPa in YAT and were outside of the range of ∼ -3.0 to 4 hPa in HYY. This indicated a relatively high sensitivity to daily residual changes in VPD, particularly in YAT. This makes sense, given that seasonal VPD in YAT is already on average above 10 hPa during the productive season, so any marginal increase above the seasonal level represents particularly warm and dry conditions. We found that extremely high VPD_R (see VPD_R>10 hPa marked by red markers in Fig.6c,d) which clearly elicited only a negative response in NEP_R (Fig.6f1,f2) consistently outweighed any positive contributions from SW_R in HYY, however the effect was mitigated in YAT when SWC_R III was seasonally high (see period delineated by red dashed lines). In both forests, high VPD_R events coincided with gaps in rainfall events of 5 mm or greater.

3.5.2 SW_R contribution towards NEP_R consistent with light response curve

NEP_R exhibited a saturated exponential response to SW_R in both forests, demonstrated by this variable's strong contribution to NEP_R (Fig.5e1,e2), that was consistent with a light-response curve despite the removal of seasonal structure (Fig.7,0,1). This suggests that NEP is acclimated to the seasonal SW radiation cycle, since a residual change in SW radiation ultimately elicits the same response in NEP_R regardless of the month in the productive season.

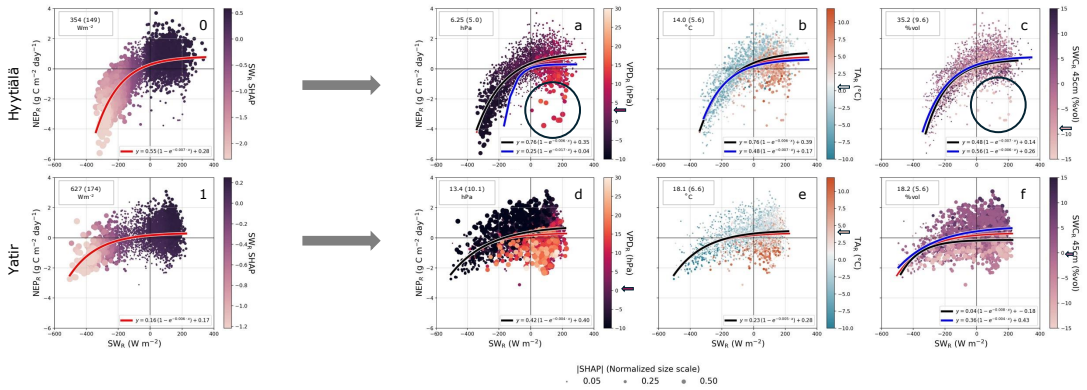

Figure 7: The influence of the main residual controlling factors on peak daily NEP_R in HYY (top row) and YAT (bottom row). Subplots 0 and 1 show the baseline relationship (red curve) between NEP_R and SW_R in HYY and YAT, respectively, while for the same reference data, a-b-c and d-e-f show how the effect of high VPD_R and TA_R and low SWC_R III (above/below thresholds determined in section 3.4) modulate this baseline relationship in HYY and YAT, respectively (the value of VPD_R, TA_R and SWC_R III are given by their respective colour bar). The size of each point represents the relative magnitude of influence of a respective variable on NEP_R (by normalized absolute SHAP value). Mean seasonal values for each factor (with standard deviation) is given in the top left corner of each subplot, for context. The black curve is the result of a shift in the baseline (red) relationship when including only data below a stress threshold, and the blue line is the shift related to data above a stress threshold. The thresholds are: VPD_R=3.6&1.0 hPa; TA_R=0.8&4.3 °C; SWC_R III=-7.8&0.0 %vol in HYY&YAT, respectively.

Building from the NEP_R-SW_R curves in Figure 70,1, we tested the sensitivity of these relationships under high VPD_R and TA_R and low SWC_R III conditions, using the respective thresholds determined in 3.4 (conditions below thresholds are modelled in black, and above thresholds in blue, Fig.7). Under intense climatic and environmental conditions, the exponential relationship was maintained while the coefficients for the formulas changed (except for VPD_R and TA_R in YAT where there were too few instances of data to fit a curve).

In HYY, high VPD_R had the strongest influence on this relationship, reducing peak NEP_R by 55% (0.55 to 0.25 g-C $m^{-2}\,day^{-1}$). SWC_R III (Fig.7c) had little effect in HYY, however, there was a compounding effect of low SWC_R III with high VPD_R evident in the larger scatter points in VPD_R during soil drought (highlighted in Fig.7a,c). In YAT, high VPD_R conditions limited peak NEP_R by 62% (0.42 to 0.16 g-C $m^{-2}\,day^{-1}$), whereas low SWC_R III (Fig.7f) dominated with a 75% reduction, bringing peak NEP_R to nearly 0 g-C $m^{-2}\,day^{-1}$. Therefore, under low SWC_R III, any additional stress (for example, high VPD_R or low SW_R conditions) would instantly subtract from the forest's total seasonal productivity.

3.5.3 Timing of residual control

Next, we tested the contribution of the main controlling residual variables throughout the months of the productive season to determine timing of potential sensitivity. We divided the residual SHAP values for each variable according to seasons with statistically high and low total NEP, and compared the median monthly SHAP values of each group against baseline forest activity (see description in A5).

In HYY, low-productivity months reflected lower positive contributions from SW_R, TA_R and VPD_R rather than strong negative controls, whereas in YAT low productivity coincided with persistent negative influence from SWC_R III when deep soil moisture failed to exceed threshold, shortening the effective growing season by up to one month. There were no particularly sensitive months in either forest; sensitivity to these variables existed throughout the season.

Positive SWC_R III had a strong contribution, though, to high-productivity months in YAT, and grossly overcame the negative influence of high VPD_R that is typical in April, the month with peak heatwave activity. Surprisingly, statistically high SWC_R III was not associated with significantly high monthly rainfall in any month, and median rainfall amount in these months was almost always less than the baseline. In HYY, there was no clear variable driving statistically high productivity over all months of the productive season, suggesting perhaps that factors outside of the scope of this study may be contributing to enhanced productivity in the forest, such as CO_2 enrichment or other broad-scale atmospheric or environmental changes.

4 Discussion

4.1 Scale-dependent climate drivers

By separating seasonal and residual variability under PAR-saturated conditions, we reveal a scale-dependent hierarchy of controls: slow hydrological boundary conditions determine seasonal carbon uptake, while atmospheric forcings dominate short-term fluctuations. This framework resolves a long-standing ambiguity in identifying dominant drivers, which are often converged across timescales in previous studies.

Seasonally, restricting the analysis to PAR-saturated conditions inadvertently challenged the conventional expectation that the "energy-limited" system, the Boreal forest, should be primarily controlled by incoming shortwave radiation. Instead, upon comparing the contrasting sites on a more equivalent basis through their productive seasons in 3.1.1, we found that Hyytiälä experiences more hours of PAR-saturated daylight than the semi-arid Yatir forest, which has substantially higher radiation on an annual basis. The latter, constrained by a prolonged summer drought that

shifts the productive season to winter-spring (Wang et al., 2020), receives then fewer daylight hours during this period, though these hours are characterized by higher radiation intensity. In this context, shortwave radiation emerges not as the dominant seasonal control but rather as a driver of short-term variability, primarily through its modulation by cloud cover and the associated rainfall regime (6c,d).

By applying PAR-saturated conditions, we effectively removed the geometric constraint imposed by solar angle and site latitude on incident radiation, allowing the analysis to focus on environmental and other atmospheric forcings across multiple timescales, ultimately revealing a consistent hydrological control of seasonal NEP discussed more in 4.2, a diverging regulation of short-term atmospheric stress (4.3) yet consistent phenological adjustment to air temperature (4.4) in the two biomes. Although long-term increases in atmospheric CO_2 and temperature are expected to influence forest carbon uptake, our results indicate that, at the timescales examined here, these effects are strongly modulated by hydrological constraints and atmospheric demand.

4.2 Interpreting seasonal controlling factors P and SWC III

Rainfall mainly influences NEP_S as a proxy, either by reducing direct radiation or increasing soil available water. In HYY, peak SWC occurred at the beginning of the productive season after snow-melt and continually decreased thereafter, despite growing inputs from precipitation (Fig.3), suggesting an indirect contribution from P_S to ET at the seasonal scale. This contrasted with YAT, where we found similar seasonality between SWC_S and NEP_S tied to a critical moisture level that controlled seasonal and residual productivity. Further to its contribution to the water balance in HYY, we considered that P_S may have also acted as a proxy for the increase in diffuse shortwave radiation (SW_{DIF}), which has a positive effect on productivity.

4.2.1 Boreal Forest and P_S

4.2.1.1 The role of seasonal rainfall in maintaining soil-water content

Precipitation supports ET and NEP by maintaining SWC and accessible soil-water for uptake. We see this seasonally in HYY, indirectly, where SWC_S in the deeper layers decreased by up to 20 %vol from April to August, in which time rainfall in the hydrologic season and productivity both peaked (3.1.2). P_S became a critical component during this time, preventing SWC_S from reaching soil-drought levels (Jauhiainen, 2004), despite higher demand than supply.

To test if the seasonal values of P_S, SWC_S and ET_S were proportional (Fig.8a), we considered previously estimated water balances in HYY (Ilvesniemi et al., 2010; Launiainen et al., 2015), where roughly 70-80% of P was found to be lost as ET and remaining 20% was lost through subsurface runoff. We found a good agreement between the sum of the cumulative values (Fig.8b) within the

period that SWC is decreasing, within which rainfall (Prec.*, 80% of P_S) cumulatively accounts for 223 mm of the total 400 mm of seasonal ET during this period. Therefore, starting with saturated soil in spring, P_S will then contribute on average 55% of ET_S and related NEP_S (R=0.97, A1), highlighting the importance of both full soil water recharge in the beginning of the season, and maintained rainfall input through to August, for seasonal productivity.

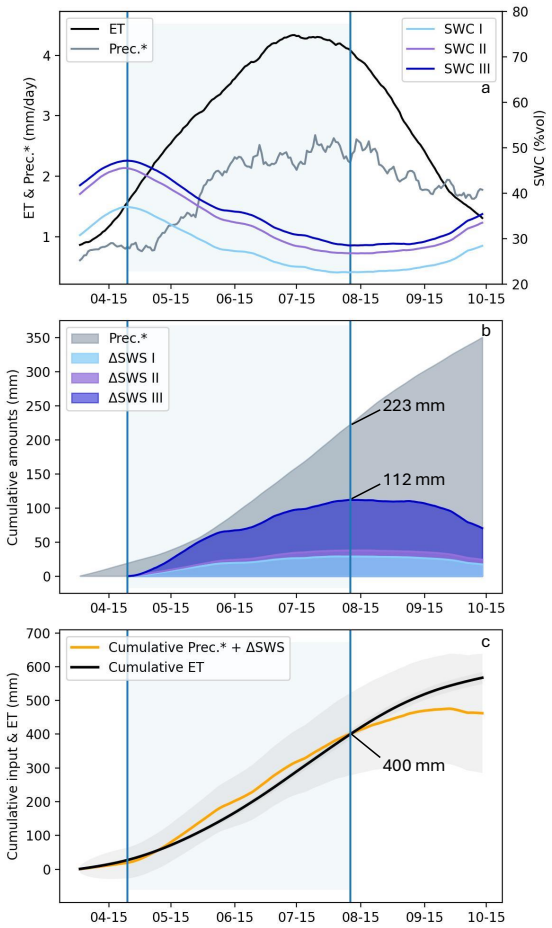

Figure 8: Estimated forest water balance in HYY. Mean seasonal ET, SWC (I-II-III) and 80% of P (Prec.*, roughly P minus runoff) are given in (a), with the cumulative sums of Prec.* and SWC (integrated over respective soil layer depth) in (b) and total sum of inputs (yellow) compared to output ET_S in (c).

4.2.1.2 Seasonal rainfall: a potential proxy for seasonal diffuse SW radiation (SW_{DIF})

SW_{DIF} is a measure of the down-welling SW radiation that has been scattered by clouds and aerosols, and is a result of atmospheric conditions that overall positively contribute to productivity in HYY. There, we found that SW_{DIF} and P_S reach a peak in seasonality along with NEP_S between June-July (Fig.3), when there is also peak activity in the forest and aerosol production that drives a net cooling forcing (Kulmala et al., 2001; Peltoniemi et al., 2015; Ezhova et al., 2018). The

combination of cloudy-rain days and boosts of aerosols during sunny days in these months explain the plateau in peak SW_{DIF} that reaches a mean ~3:4 ratio with direct SW_S, leading to relatively cooler conditions at the unique time of the year when this northern location receives up to 19.5 hours of daylight and what would be a mean daily 600 $W\,m^{-2}$ clear-sky SW radiation. Forest productivity has seemingly adapted to this 3:4 ratio, since it was found that high SW_{DIF}:SW_{DIRECT} regimes reached deeper into the canopy layers and generated the same mean rate of gross primary productivity (GPP, ecosystem carbon uptake) as SW_{DIR}, using less than half the incident PAR and from less stressful VPD conditions (Gu et al., 2002; Neimane-Šroma et al., 2024).

With the 10 years of SW_{DIF} data in HYY, we were able to calculate seasonal SW_{DIF} ($SW_{DIF,S}$) and rerun the seasonal analysis. The lead controlling factors from the SHAP analysis, however, were unchanged, likely due to inconsistency in seasonality between $SW_{DIF,S}$ and NEP_S in early spring, when atmospheric conditions contribute to maintaining relatively high SW_{DIF} under low TA_S (Kulmala et al., 2001; Sogacheva et al., 2008; Sinclair et al., 2022). Although SW_{DIF} does not emerge as a dominant independent controlling factor in the SHAP analysis, extensive prior work at HYY indicates that it covaries strongly with precipitation and contributes indirectly to seasonal productivity.

4.2.2 Semi-arid Forest: critically controlled by deep SWC

4.2.2.1 Relationship between SWC III, precipitation, and start of productive season

SWC III had a critical control on the timing, duration and magnitude of the productive season in the semi-arid Yatir site. There, rainfall is infrequent and highly variable in both amount and intensity, which influences penetration to deeper soil layers (Yaseef et al., 2010). This effect is particularly pronounced at the beginning of the wet season when the soil is dry (5.4-11.3 %vol for layers I-III), leading to a delay of roughly three weeks between the mean end of the dry season (November 11th; the average first day of rainfall greater than 5 mm) and start of the productive season (December 4th, 3.1.1); and an additional month delay before SWC_S III exceeds and remains above the critical threshold of 15.9 %vol, January 13th.

The residual NEP analysis further revealed that high variability in daily rainfall in YAT can delay the peak of productivity by one month, but that oppositely, highly productive seasons are not associated with significantly high amounts of rainfall (3.5.3). This indicates that peak productivity in YAT is initially limited by the slow process of re-wetting of the soil profile (a legacy effect from the dry season), and that rainfall quality (intensity, duration and frequency) is more pertinent than total rainfall amount.

4.2.2.2 SWC III: Physical limiting factors from dry season

The prolonged dry season depletes soil moisture through to the deepest layer, and re-wetting from rainfall creates gradients in soil moisture and potential that compete against root water uptake (Richards, 1931; Guswa et al., 2002). Early in the productive season, NEP_S is moderately supported by shallow soil moisture (layers I–II), while SWC_S III exerts a negative influence until it is replenished beyond the critical threshold (Fig. 4d). This aligns with previously reported transpirable limits of ∼16 %vol across the main soil profile and root-zone (Preisler et al., 2019), which in addition to the protective mechanism of root detachment from soil under highly negative soil-water potential (SWP), below -1.5 MPa (Nadal-Sala et al., 2024), demonstrates the main physical limitations on root water-uptake in YAT as a result of the intense dry season.

To further explore these constraints, we estimated SWP across all layers using the Van Genuchten formula (Van Genuchten, 1980) (see **??** in Supplementary Materials for more details). We found that SWP_S III rose exponentially to transpirable levels (> -1.5 MPa) concurrently with SWC_S III rising above threshold, and that it was the last layer to do so (see Fig. 9a).

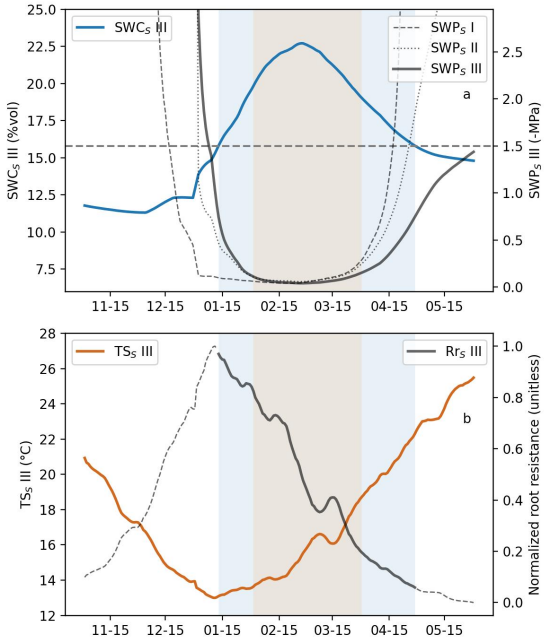

Figure 9: Seasonal changes in SWC, soil temperature (TS), soil water potential (SWP) and normalized root resistance (Rr) in soil layer III in YAT. From February to March (orange shading) SWP_S III was minimal, while Rr_S III drastically decreased by 75% (or, conductivity increased by 300%). Overall, in the peak of the productive season (blue shading), SWP_S III was less negative than the previously estimated soil potential threshold of -2.0 MPa at which complete stomatal closure is induced (Klein et al., 2014), while Rr_S III ranges from peak to minimal values.

Therefore, before SWC_S III was replenished, SWP_S III remained more negative than both the

overlying layers and the roots, creating a vertical potential gradient that draws water downward and away from the main root zone. This acts as a competing constraint on water uptake, effectively delaying productivity until deep soil moisture is replenished. The gradient was reversed, however, by the end of the productive season, with SWP_S III remaining the least negative layer above the transpirable limit. It should be noted that the mechanics and support towards transpiration in the rock layer below the soil has yet to be studied in YAT, though it is expected to support the modest transpiration fluxes during the dry season. While the largest root density is in the upper soil layers, it is also still unclear how much each layer contributes to total water uptake.

4.2.2.3 SWC III: Biological limiting factor in wet season

Once deep soil moisture is replenished, physical constraints on water uptake diminish, and root resistance becomes a dominant constraint that is largely temperature-dependent (Reicosky and Ritchie, 1976; Running and Reid, 1980; Kramer and Boyer, 1995; García-Tejera et al., 2016).

We found that, for comparable SWC amounts, there was a 13-35% lower positive contribution to NEP_S in January-February than in March-April (Fig.5a2). Since the SHAP value is specific to a respective variable, the difference must be explained by the variable itself, or a variable related to SWC and its uptake that were not inputs to the model (i.e., the difference in contribution cannot be explained, for example, by changes in air temperature in these months). Using soil temperature (TS) records in YAT, we found that TS_S III rises from a minimum $\sim$ 13 °C to 23 °C over the productive season, reducing root resistance and improving water uptake (see Fig.9b; see A6 for more details on the calculations). Notably, the rise in SWC_S III above threshold coincided with the annual minimum in soil temperature, resulting in a transitional period where uptake is limited not by water availability, but by biological constraints. Essentially, as TS increases, root conductance increases and enhances productivity, which we ultimately see reflected in the SWC_S III SHAP values.

Altogether, this demonstrates that productivity in YAT is first controlled by a physical limitation on water uptake imposed by delayed deep-soil recharge, and later by a temperature-dependent biological limitation. Combining these constraints with the observation that statistically high NEP only begins in January (Table 2), it appears that the start of the productive season in YAT has been fully optimized.

4.3 Adaptation and sensitivity to atmospheric stress

VPD sensitivity in both forests reflected a physiological adaptation to the prevailing climate, and not stress avoidance. Both ecosystems were sensitive to VPD rising above the seasonal mean, despite vastly differing historical conditions in each location. In the productive season in YAT,

peak seasonal VPD was more than double that of HYY, and high VPD reduced peak residual productivity by up to 62% in YAT and 55% in HYY (3.5.2). The negative effect from VPD in YAT, however, was mitigated by SWC III (when SWC III was sufficient), further confirming that Aleppo pine could regulate stomatal conductance under chronically high VPD (Preisler et al., 2023) given sustained root-water uptake as explained in 4.2.2.2.

In HYY, where conditions are cooler, wetter, and VPD is typically less intense, this mitigation was not observed. This can be explained by species-specific hydraulic traits, where resistivity to embolism (P50) in Scots pine across Europe showed no adaptation to atmospheric demand (Martínez-Vilalta et al., 2009), and is overall less resistant than Aleppo pine to high tension on its hydraulic system ($P50_{HYY}$=-2.89 MPa, $P50_{YAT}$=-3.95 MPa) (Martínez-Vilalta et al., 2009; Klein et al., 2016); whereas denser canopy growth (a high leaf-to-sapwood ratio) and lower leaf conductivity (low leaf-specific hydraulic conductivity) in HYY Scots pine reflected adaptation to a wet and low-VPD environment (Martínez-Vilalta et al., 2009).

With climate change, a significant increase in high VPD days could therefore have a persistent negative influence on productivity in the Boreal Hyytiälä forest, despite this not being a water-limited environment; whereas a change in the rainfall regime that replenishes deep soil moisture in the semi-arid Yatir would push the forest beyond its VPD-adapted range. In recent years, there has been an increase in the count of days with seasonally high VPD in Hyytiälä, and a continual decline in mean deep SWC in Yatir, below the critical threshold (Fig.10 a and c, respectively). While there is no perceptible change in total NEP in Hyytiälä in the productive season in response to VPD, productivity in Yatir is declining, and potentially becoming more vulnerable to days with high VPD, which account for more than 50 out of the mean 175 day productive season.

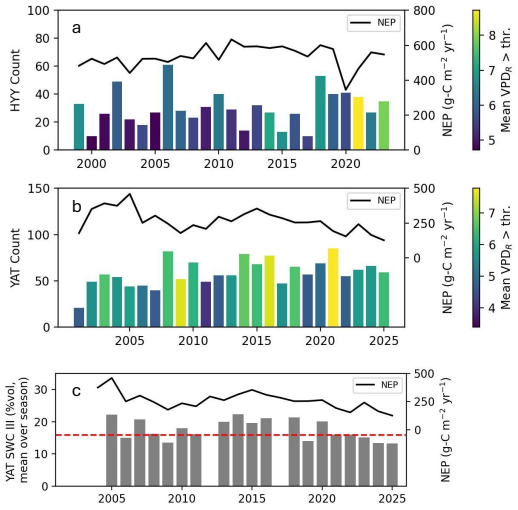

Figure 10: Count of high VPD events per season (VPD_R > thresholds determined in 3.4), in (a) HYY and (b) YAT, with total productive season NEP (black line). Bar colour indicates the mean of the counted VPD_R. For YAT, mean productive season SWC III is given in (c) with the 15.9 %vol SWC threshold (red-dashed line), to reflect the seasons when SWC III was low and when the forest was resultingly more sensitive to high VPD. The drop in NEP in HYY in 2020-2021 is a result of intense forest thinning (Aslan et al., 2024).

The observed shifts in VPD frequency in Hyytiälä and declining deep soil moisture in Yatir suggest that the identified controls are not static, but are already evolving under changing climate conditions. In Hyytiälä, the increasing frequency of high VPD events (defined relative to the residual thresholds in Section 3.4, seen in Fig.10a) indicates a shift toward more frequent atmospheric stress conditions during the productive season. In contrast, no clear long-term trend in total productive season precipitation was observed (see Supplementary Materials, **??**), suggesting that changes in atmospheric demand may increasingly decouple from water supply. In Yatir, mean deep soil water content (SWC III) shows a declining tendency over time, with multiple recent years falling below the identified threshold of 15.9 %vol (Fig.10c). This indicates an increasing frequency of seasons in which deep soil moisture fails to reach levels required for sustained productivity. Notably, this decline is not directly explained by total rainfall amounts, reinforcing the importance of rainfall regime characteristics (timing, intensity, and infiltration) rather than annual totals alone.

4.4 Convergent thermal optimum

Peak seasonal productivity in the two contrasting regions was tuned to a similar optimal temperature range of ∼ 14-20 °C, that was consistent with observations from comparable forests and climatic conditions (Rotenberg and Yakir, 2010; Huang et al., 2019; Bennett et al., 2021).

This convergence reflects an underlying physiological constraint on photosynthesis that is preserved across both biomes. Rather than adjusting their intrinsic physiological temperature optima over a multi-decade period, the forests appear to adjust the timing of peak productivity to coincide with this favourable temperature range, given sufficient soil moisture. In this sense, forest response primarily reflects shifts in phenology rather than physiology, harmonizing the productive season against temperature and rainfall regime constraints (Wang et al., 2020), even across hydroclimatic extremes.

This interpretation is supported by the relatively wide flexibility in the timing of the productive seasons over the 25 year records (3.1.1), compared to the limited plasticity in temperature optima reported for photosynthesis of approximately 0.34-0.37 °C per degree of warming (Sendall et al., 2015; Crous et al., 2022). This adjustment is partial and moreover does not necessarily preserve carbon assimilation rates, particularly in warmer climates, where reductions in leaf nitrogen, photosynthetic capacity, and increased stomatal limitations from warming constrain carbon uptake (Crous et al., 2022).

Altogether, the results suggest that under climate change, changes in hydrological regimes, through their control over the seasonality of productivity and its plasticity, will likely a have stronger influence on forest carbon uptake than gradual shifts in mean temperature. This study is based on two end-member ecosystems and therefore does not aim to establish universal relationships across all forest types. Instead, it provides a process-based comparison across hydroclimatic extremes. In addition, while the explainable machine learning framework identifies dominant statistical controls consistent with physical mechanisms, it does not establish causality. Extending this approach to additional sites and integrating process-based models would further strengthen generalization.

5 Implications

This study compared rare long-term bi-continental records of forest productivity in two contrasting ecosystems, the Boreal Hyytiälä forest and the semi-arid Yatir forest. To address the complexity of these datasets, we applied SHAP analysis to interpret machine learning model outputs, following rigorous validation to mitigate the "black-box" nature of the models and ensure physically consistent results.

The results reveal a scale-dependent hierarchy of controls on forest productivity. At the seasonal scale, regional hydrological regimes dominate, governing productivity through soil water replenishment and, indirectly, through modulation of diffuse radiation (SW_{DIF}). A broadly consistent air temperature optimum was also observed across both forests, suggesting a conserved physiological constraint, though temperature exerted a comparatively weaker influence on NEP.

At the daily scale, VPD emerges as a critical and additive control on NEP. Its influence, however, should not necessarily imply water limitation in the system: in the Boreal Hyytiälä, strong VPD sensitivity occurs despite ample water availability. In the semi-arid Yatir, VPD is mitigated by adequate soil moisture, though the effect is highly constrained.

In semi-arid forests in particular, which experience prolonged dry seasons that impose strong limitations on productivity, incorporating deeper soil layers into mechanistic ecohydrological frameworks is essential for explaining both the magnitude of carbon uptake and the timing of the productive season. Rainfall totals alone are insufficient, given the complex process of soil-layer re-wetting from few and highly-variable rainfall events. Soil moisture thresholds play a central role in defining seasonal boundaries, shifting the productive season to relatively energy-limited conditions, and challenging the simple classification of forests based on plant functional type.

Acknowledgements

This project was supported by ISF-BRG grant 2481/22, and by grants from the Kimmel Center for Planetary Sciences, and the Institute for Environmental Sustainability (IES) at the Weizmann Institute of Science.

It was also supported by ICOS Finland and by University of Helsinki.

ET was funded by NSF grant 2303486 from the P4CLIMATE program of the Geosciences (GEO) Directorate and by Harvard Dean's Competitive Fund for Promising Scholarship, and thanks the Weizmann Institute for its hospitality during parts of this work.

This work was supported by the AI Hub at the Institute for Artificial Intelligence, Weizmann Institute of Science.

Laura Rez was supported by the Samuel G. Rose Environmental Sustainability Fellows Fund as part of the Institute for Environmental Sustainability (IES) at the Weizmann Institute of Science.

Declaration of interests

The authors declare no competing interests.

Appendix

A1 Dataset correlations and clustering

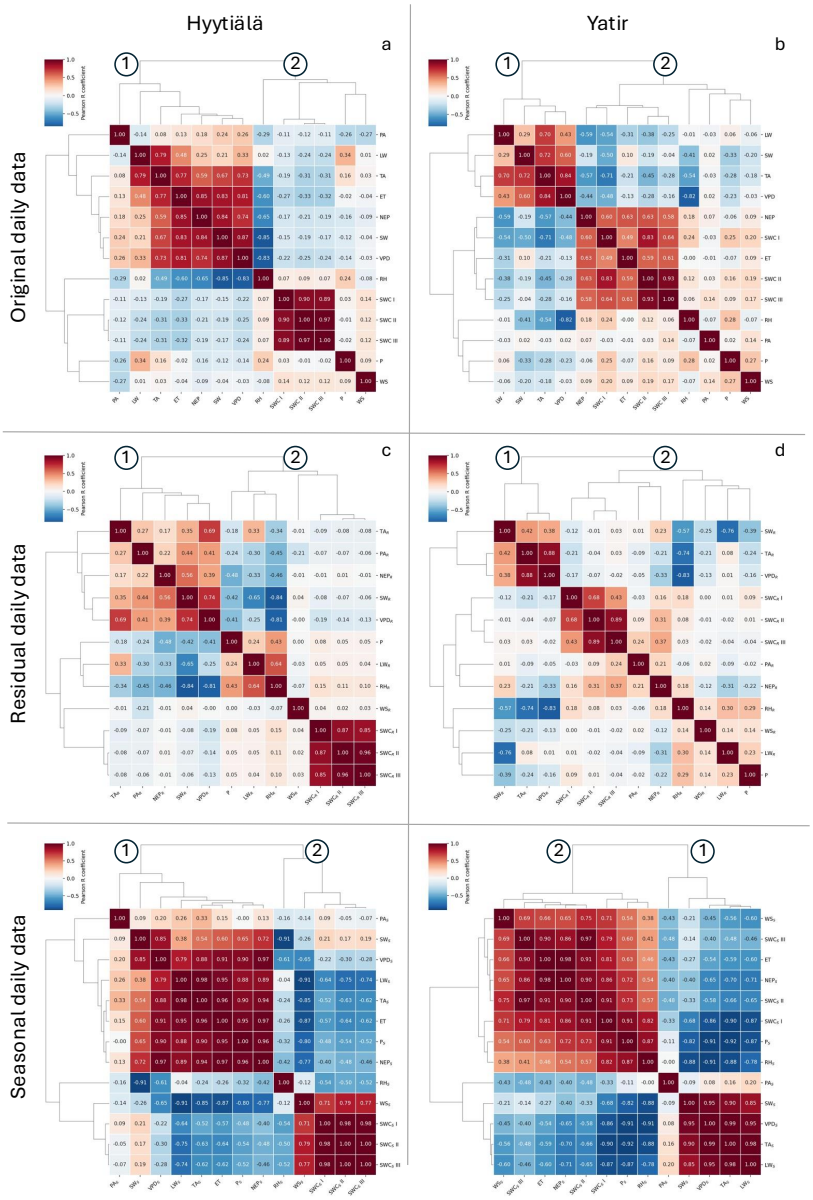

Figure A1: Hierarchal clustering of feature correlations in the original (a, b) and residual (c, d) datasets for each forest (HYY:a, c; YAT:b, d). In nearly each dataset, there are two clear groupings of features: Group 1, containing shortwave radiation (SW) and the variables commonly related to it, directly or indirectly: TA, VPD and LW; and Group 2, factors related to precipitation (P, PA, RH, SWC, WS). NEP and ET are correlated and clustered together in the original datasets, however they are grouped into Group 1 in HYY and Group 2 in YAT. In both forests, SWC at 30 cm and 45 cm are closely correlated, while this correlation becomes much weaker with the top 15 cm layer in YAT.

A2 Yatir model predictions and scores

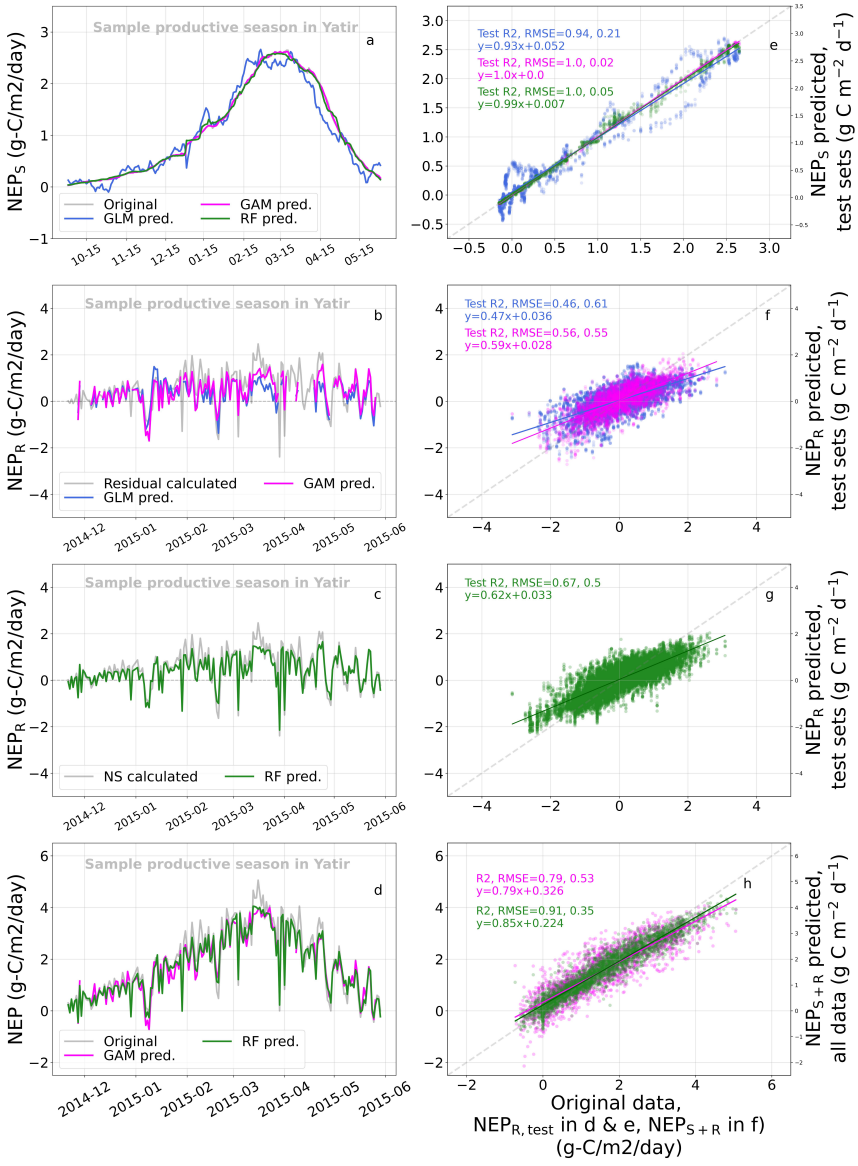

Figure A2: Model performances in predicting NEP for YAT (similar figure for HYY can be found in A3). The left column shows the predictions for a sample productive season (2014-2015), while the right column gives the test and whole dataset predictions for 20 random seeds (the test set is 10% of the whole dataset). NEP_S is relatively well-predicted by all models (a, e; R^2_{test}=0.94;1.0;1.0 for GLM;GAM;RF, respectively). GLM and GAM (b, f) predict NEP_R at a lower accuracy (R^2_{test}=0.46&0.56, respectively) than RF (c, g; R^2_{test}=0.67), particularly for negative NEP_R, where results are highly scattered in GLM and GAM. Learning residual data with RF separate from the seasonal cycle resulted in a strong performance in the combined NEP prediction than GAM (R^2=0.91&0.79 for RF&GAM, respectively), and ensured that the strong seasonal cycle would not dominate the outputs from the SHAP analysis on controlling factors.

A3 Hyytiälä model predictions and scores

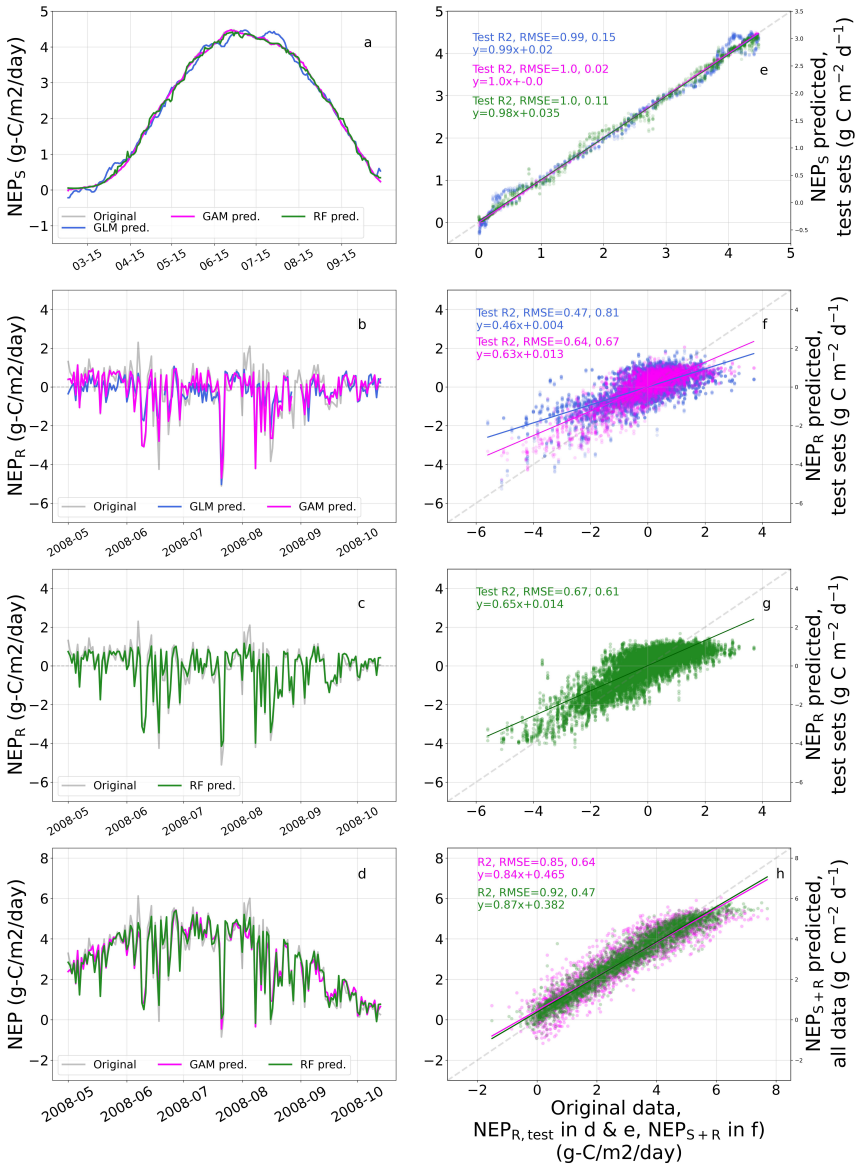

Figure A3: Model performances in predicting NEP for HYY. The left column shows the predictions from a sample productive season in 2008, while the right column shows test- and whole data-set predictions for 20 random seeds. GLM and GAM (a, d) predict peripheral residual values at a lower accuracy (test R^2 & RMSE of 0.57, 0.93 and 0.63, 0.86, respectively) than RF (b, e; test R^2 & RMSE of 0.66, 0.83). The slight improvement in model learning for NEP_R from GAM to RF translated to a important improvement over the entire dataset (f) where R^2 increased by 0.11, RMSE reduced by 0.23.

A4 Cleaning and testing with ML

To test that the RF model was indeed learning structure in the residual dataset and not random noise, we cleaned layers of month-years that were obvious outliers by their Z-scores

and performed a permutation test (see Fig.A4). This test, in which the target NEP_R values are randomly shuffled while keeping the feature data the same, was run on 1000 random seeds and resulted in a small distribution of R^2_{test} next to zero, in both forests (for example in YAT, $R^2_{\text{residual (perm.) test, YAT}}$= 1.5e-4 (STD=0.0012). This greatly varied from the true values ($R^2_{\text{residual (true) test}}$=0.66 (STD=0.019), and proved that the RF model learned actual structure from the residual datasets.

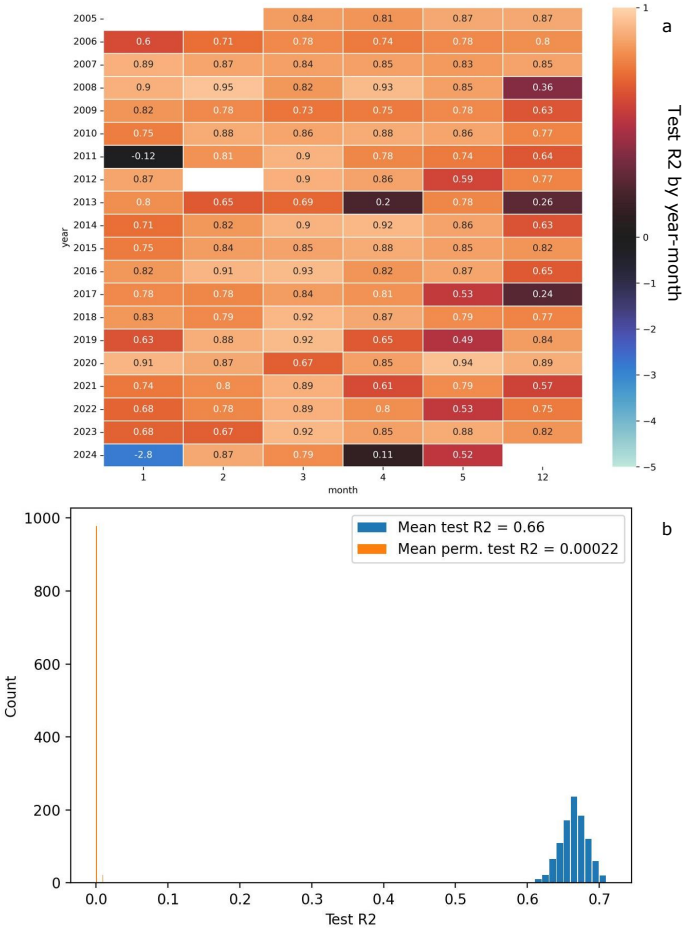

Figure A4: The test R2 (predictions using 10% of unseen data to the models) from 20 random seeds on YAT residual data, presented in (a) by mean month-year, and in (b) as the distribution from a permutation test. From (a), it can be seen that 2024-01, for example, is an outlier month that the model could not learn well; this was indeed a period with a poor NEP record. Removing specific year-months then improved, in turn, model training and the resulting test R2 of other year-months. In (b), the permutation test shows that the RF model has learned relationships within the original residual data as it has a vastly different distribution from the output of the models trained on randomly shuffled target values (i.e., containing random "noise" relationships). This shows that while residual data certainly contains some amount of noise, there are relationships that aren't random for the RF model to learn.

A5 Median monthly SHAP contributions to NEP_R

Table 2: Median NEP_R and median SHAP values of main controlling factors by month in YAT, for seasons grouped by low (bottom 25th percentile), mid (25th-75th percentile), and high (top 75th percentile) total NEP. Statistically significant median values (evaluated against mid group, $p<0.05$) are denoted in bold with '*'. Median SWC_R III monthly SHAP values are underlined for months when, in given percentile years, mean SWC III was below 15.8 %vol. **Low years**: 2008, 2009, 2010, 2019; **Baseline years**: 2006, 2011, 2012, 2013, 2016, 2017, 2018, 2020; **High years**: 2005, 2007, 2014, 2015.

	Dec.	Jan.	Feb.	Mar.	Apr.	May
NEP_R	**-0.23*** /0.27/0.16	**-0.40*** /0.17/**0.62***	**-0.76*** /0.23/**0.70***	**-0.30*** /-0.081/**0.85***	**-0.64*** /0.034/**0.72***	**-0.42*** /-0.16/**0.49***
SW_R	0.13/0.14/0.14	0.13/14/**0.19***	**0.12*** /0.17/**0.19***	**0.12*** /0.15/**0.18***	**0.080*** /0.080/**0.14***	**0.070*** /0.080/**0.11***
VPD_R	-0.006/0.014/**0.054***	0.016/0.029/0.000	**0.005*** /0.019/0.046	0.087/0.036/**0.075***	**-0.005*** /0.105/**-0.006***	0.008/0.007/**0.11***
TA_R	0.005/0.005/**-0.002***	**0.000*** /0.005/0.008	**-0.004*** /0.007/0.011	**-0.011*** /0.003/0.001	**-0.014*** /0.001/-0.004	0.001/0.002/0.005
SWC_R III	**-0.19*** /0.11/**-0.094***	**-0.31*** /0.071/**0.21***	**-0.22*** /0.14/**0.23***	**-0.20*** /-0.003/**0.28***	**-0.26*** /-0.006/**0.35***	**-0.19*** /0.045/**0.34***
P	25.7/48.9/22.6	**29.6*** /81.9/52.4	61.2/48.8/38.0	29.1/24.7/44.1	3.1/14.7/10.1	**0.2*** /3.0/9.7

Table 3: Same as Table 2 but for HYY. **Low years**: 1999, 2001, 2003, 2004, 2006; **Baseline years**: 1997, 1998, 2000, 2002, 2005, 2007, 2008, 2010, 2014, 2016, 2017; **High years**: 2009, 2011, 2012, 2013, 2015..

	Apr.	May	Jun.	Jul.	Aug.	Sep.
NEP_R	0.027/0.19/0.27	**-0.16***/0.058/**0.46***	**-0.056***/0.23/**0.76***	-0.12/0.071/**0.97***	**-0.12***/0.33/**0.66***	**0.11***/0.26/0.19
SW_R	0.32/0.33/0.31	0.25/0.32/0.36	0.35/0.34/0.36	0.40/0.34/0.27	0.31/0.34/0.41	0.35/0.38/**0.092***
VPD_R	**0.032***/0.039/0.038	0.025/0.025/**0.057***	**0.018***/0.032/**0.057***	0.022/0.028/**0.047***	**0.024***/0.038/**0.047***	0.032/0.036/**0.047***
TA_R	0.005/-0.001/**0.017***	0.031/0.015/0.013	0.012/0.027/**0.050***	0.0013/0.022/**0.060***	**0.007***/0.031/0.015	**-0.019***/0.024/**-0.001***
SWC_R III	**-0.015***/-0.004/0.003	**-0.012***/0.002/**0.019***	**-0.019**/-0.004/**0.022***	**-0.019***/-0.005/**0.018***	**-0.017***/-0.005/**0.019***	**-0.018***/-0.004/-0.008
P	23.7/33.7/38.8	50.9/53.3/43.4	63.6/91.1/94.7	67.3/93.6/91.7	**48.4***/104.4/62.4	71.6/47.2/79.8

A6 Estimating soil layer III temperature and root resistance

While there are continuous ∼ 20 year soil temperature measurements for layers I & II, layer III - which is key for the analysis, has less than 5 years on record. Soil temperature in layer II and III are steady measurements that are strongly correlated, as seen in Figure A5, and therefore the regression formula between the two overlapping measurements (SWC_{III}=0.82 SWC_{II} + 3.55) was used to estimate layer III for the 20 year period.

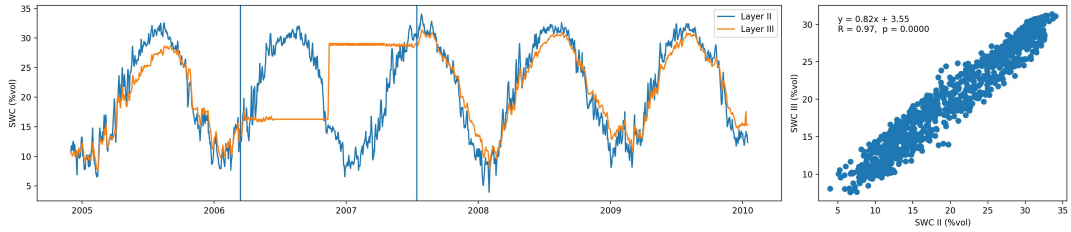

Figure A5: Overlapping period of soil temperature measurements in YAT in layer II & III (left), and the correlation and regression results of the measurements (excluding values between 2006/03/15 and 2007/07/15, dates highlighted by vertical lines).

We estimated root resistance using the formula obtained from García-Tejera et al. (2016), and averaged parameters. The goal was to illustrate the Arrhenius-type relationship between root resistance and soil temperature, and since we do not have the specific parameters for this forest, we only present normalized values.

References

Anderson, K., Hansen, C. W., Holmgren, W. F., Jensen, A., Mikofski, M. A. and Driesse, A. (2023), 'pvlib python: 2023 project update', *Journal of Open Source Software* **8**(92), 5994.

Appiagyei, B. D., Belhoucine-Guezouli, L., Bessah, E., Morsli, B. and Fernandes, P. A. M. (2022), 'A review on climate change impacts on forest ecosystem services in the mediterranean basin', *Journal of Landscape Ecology* **15**(1), 1–26.

Aslan, T., Launiainen, S., Kolari, P., Peltola, O., Aalto, J., Bäck, J., Vesala, T. and Mammarella, I. (2024), 'Thinning turned boreal forest to a temporary carbon source-short term effects of partial harvest on carbon dioxide and water vapor fluxes', *Agricultural and Forest Meteorology* **353**, 110061.

Bartsch, S., Stegehuis, A., Boissard, C., Lathière, J., Peterschmitt, J.-Y., Reiter, I., Gauquelin, T., Baldy, V., Genesio, L., Matteucci, G. et al. (2020), 'Impact of precipitation, air temperature and

abiotic emissions on gross primary production in mediterranean ecosystems in europe', *European Journal of Forest Research* **139**(1), 111–126.

Beer, C., Reichstein, M., Tomelleri, E., Ciais, P., Jung, M., Carvalhais, N., Rödenbeck, C., Arain, M. A., Baldocchi, D., Bonan, G. B. et al. (2010), 'Terrestrial gross carbon dioxide uptake: global distribution and covariation with climate', *Science* **329**(5993), 834–838.

Bennett, A. C., Arndt, S. K., Bennett, L. T., Knauer, J., Beringer, J., Griebel, A., Hinko-Najera, N., Liddell, M. J., Metzen, D., Pendall, E. et al. (2021), 'Thermal optima of gross primary productivity are closely aligned with mean air temperatures across australian wooded ecosystems', *Global Change Biology* **27**(19), 4727–4744.

Böttcher, K., Aurela, M., Kervinen, M., Markkanen, T., Mattila, O.-P., Kolari, P., Metsämäki, S., Aalto, T., Arslan, A. N. and Pulliainen, J. (2014), 'Modis time-series-derived indicators for the beginning of the growing season in boreal coniferous forest—a comparison with co2 flux measurements and phenological observations in finland', *Remote Sensing of Environment* **140**, 625–638.

Cernusak, L. and Marshall, J. (2000), 'Photosynthetic refixation in branches of western white pine', *Functional Ecology* **14**(3), 300–311.

Crous, K. Y., Uddling, J. and De Kauwe, M. G. (2022), 'Temperature responses of photosynthesis and respiration in evergreen trees from boreal to tropical latitudes', *New Phytologist* **234**(2), 353–374.

Curtis, P. S. and Gough, C. M. (2018), 'Forest aging, disturbance and the carbon cycle', *New Phytologist* **219**(4), 1188–1193.

Estiarte, M., Vicca, S., Peñuelas, J., Bahn, M., Beier, C., Emmett, B. A., Fay, P. A., Hanson, P. J., Hasibeder, R., Kigel, J. et al. (2016), 'Few multiyear precipitation–reduction experiments find a shift in the productivity–precipitation relationship', *Global change biology* **22**(7), 2570–2581.

Ezhova, E., Laanti, T., Lintunen, A., Kolari, P., Nieminen, T., Mammarella, I., Heljanko, K. and Kulmala, M. (2025), 'Explainable machine learning for modeling of net ecosystem exchange in boreal forests', *Biogeosciences* **22**(1), 257–288.

Ezhova, E., Ylivinkka, I., Kuusk, J., Komsaare, K., Vana, M., Krasnova, A., Noe, S., Arshinov, M., Belan, B., Park, S.-B. et al. (2018), 'Direct effect of aerosols on solar radiation and gross primary production in boreal and hemiboreal forests', *Atmospheric Chemistry and Physics* **18**(24), 17863–17881.

Food and Agriculture Organization of the United Nations and UNESCO (1990), 'Title of the publication'.

García-Tejera, O., López-Bernal, Á., Villalobos, F. J., Orgaz, F. and Testi, L. (2016), 'Effect of soil temperature on root resistance: implications for different trees under mediterranean conditions', *Tree Physiology* **36**(4), 469–478.

Gu, L., Baldocchi, D., Verma, S. B., Black, T., Vesala, T., Falge, E. M. and Dowty, P. R. (2002), 'Advantages of diffuse radiation for terrestrial ecosystem productivity', *Journal of Geophysical Research: Atmospheres* **107**(D6), ACL–2.

Guswa, A. J., Celia, M. A. and Rodriguez-Iturbe, I. (2002), 'Models of soil moisture dynamics in ecohydrology: A comparative study', *Water Resources Research* **38**(9), 5–1.

Hammond, W. M., Williams, A. P., Abatzoglou, J. T., Adams, H. D., Klein, T., López, R., Sáenz-Romero, C., Hartmann, H., Breshears, D. D. and Allen, C. D. (2022), 'Global field observations of tree die-off reveal hotter-drought fingerprint for earth's forests', *Nature communications* **13**(1), 1761.

Han, J., Guo, C., Ye, S., Zhang, L., Li, S., Wang, H. and Yu, G. (2020), 'Effects of diffuse photosynthetically active radiation on gross primary productivity in a subtropical coniferous plantation vary in different timescales', *Ecological Indicators* **115**, 106403.

Hari, P., Kulmala, M., Pohja, T., Lahti, T., Siivola, E., Palva, L., Aalto, P., Hämeri, K., Vesala, T., Luoma, S. et al. (1994), 'Air pollution in eastern lapland: challenge for an environmental measurement station.'.

Hättenschwiler, S., Miglietta, F., Raschi, A. and Körner, C. (1997), 'Thirty years of in situ tree growth under elevated co2: a model for future forest responses?', *Global Change Biology* **3**(5), 463–471.

Huang, M., Piao, S., Ciais, P., Peñuelas, J., Wang, X., Keenan, T. F., Peng, S., Berry, J. A., Wang, K., Mao, J. et al. (2019), 'Air temperature optima of vegetation productivity across global biomes', *Nature ecology & evolution* **3**(5), 772–779.

Hubau, W., Lewis, S. L., Phillips, O. L., Affum-Baffoe, K., Beeckman, H., Cuní-Sanchez, A., Daniels, A. K., Ewango, C. E., Fauset, S., Mukinzi, J. M. et al. (2020), 'Asynchronous carbon sink saturation in african and amazonian tropical forests', *Nature* **579**(7797), 80–87.

Ilvesniemi, H., Pumpanen, J., Duursma, R., Hari, P., Keronen, P., Kolari, P., Kulmala, M., Mammarella, I., Nikinmaa, E., Rannik, Ü. et al. (2010), 'Water balance of a boreal scots pine forest', *Boreal Environment Research* **15**(4), 375.

IPCC (2023), *Climate Change 2022: Impacts, Adaptation and Vulnerability*, Cambridge University Press. Contribution of Working Group II to the Sixth Assessment Report of the Intergovernmental Panel on Climate Change.

Jauhiainen, M. (2004), *Relationships of particle size distribution curve, soil water retention curve and unsaturated hydraulic conductivity and their implications on water balance of forested and agricultural hillslopes*, Helsinki University of Technology.

Klein, T., Cohen, S., Paudel, I., Preisler, Y., Rotenberg, E. and Yakir, D. (2016), 'Diurnal dynamics of water transport, storage and hydraulic conductivity in pine trees under seasonal drought', *iForest-Biogeosciences and Forestry* **9**(5), 710.

Klein, T., Rotenberg, E., Cohen-Hilaleh, E., Raz-Yaseef, N., Tatarinov, F., Preisler, Y., Ogée, J., Cohen, S. and Yakir, D. (2014), 'Quantifying transpirable soil water and its relations to tree water use dynamics in a water-limited pine forest', *Ecohydrology* **7**(2), 409–419.

Kong, Z., Wang, T., Han, Q., Dai, Y., Wang, L. and Chen, X. (2022), 'Evaluation of environmental controls on terrestrial net ecosystem exchange of co2: A global perspective from the fluxnet sites', *Journal of Geophysical Research: Atmospheres* **127**(22), e2022JD037217.

Kramer, P. J. and Boyer, J. S. (1995), *Water relations of plants and soils*, Academic press.

Kulmala, M., Hämeri, K., Aalto, P., Mäkelä, J., Pirjola, L., Nilsson, E. D., Buzorius, G., Rannik, Ü., Dal Maso, M., Seidl, W. et al. (2001), 'Overview of the international project on biogenic aerosol formation in the boreal forest (biofor)', *Tellus B* **53**(4), 324–343.

Launiainen, S., Katul, G. G., Lauren, A. and Kolari, P. (2015), 'Coupling boreal forest co2, h2o and energy flows by a vertically structured forest canopy–soil model with separate bryophyte layer', *Ecological modelling* **312**, 385–405.

Leverenz, J. W. (1987), 'Chlorophyll content and the light response curve of shade-adapted conifer needles', *Physiologia plantarum* **71**(1), 20–29.

Li, Y., Zhang, Y. and Lv, J. (2022), 'Interannual variations in gpp in forest ecosystems in southwest china and regional differences in the climatic contributions', *Ecological Informatics* **69**, 101591.

Lundberg, S. (2017), 'A unified approach to interpreting model predictions', *arXiv preprint arXiv:1705.07874* .

Mäkelä, A., Kolari, P., Karimäki, J., Nikinmaa, E., Perämäki, M. and Hari, P. (2006), 'Modelling five years of weather-driven variation of gpp in a boreal forest', *Agricultural and Forest Meteorology* **139**(3-4), 382–398.

Markos, N., Preisler, Y., Radoglou, K., Rotenberg, E. and Yakir, D. (2024), 'Physiological and phenological adjustments in water and carbon fluxes of aleppo pine forests under contrasting climates in the eastern mediterranean', *Tree Physiology* **44**(1), tpad125.

Marshall, B. and Biscoe, P. (1980), 'A model for c3 leaves describing the dependence of net photosynthesis on irradiance', *Journal of Experimental Botany* **31**(1), 29–39.

Martínez-Vilalta, J., Cochard, H., Mencuccini, M., Sterck, F., Herrero, A., Korhonen, J., Llorens, P., Nikinmaa, E., Nole, A., Poyatos, R. et al. (2009), 'Hydraulic adjustment of scots pine across europe', *New Phytologist* **184**(2), 353–364.

Nadal-Sala, D., Grote, R., Kraus, D., Hochberg, U., Klein, T., Wagner, Y., Tatarinov, F., Yakir, D. and Ruehr, N. K. (2024), 'Integration of tree hydraulic processes and functional impairment to capture the drought resilience of a semi-arid pine forest', *Biogeosciences Discussions* **2023**, 1–35.

Neimane-Šroma, S., Durand, M., Lintunen, A., Aalto, J. and Robson, T. M. (2024), 'Shedding light on the increased carbon uptake by a boreal forest under diffuse solar radiation across multiple scales', *Global Change Biology* **30**(4), e17275.

Pan, Y., Birdsey, R. A., Phillips, O. L., Houghton, R. A., Fang, J., Kauppi, P. E., Keith, H., Kurz, W. A., Ito, A., Lewis, S. L. et al. (2024), 'The enduring world forest carbon sink', *Nature* **631**(8021), 563–569.

Park, T., Chen, C., Macias-Fauria, M., Tømmervik, H., Choi, S., Winkler, A., Bhatt, U. S., Walker, D. A., Piao, S., Brovkin, V. et al. (2019), 'Changes in timing of seasonal peak photosynthetic activity in northern ecosystems', *Global Change Biology* **25**(7), 2382–2395.

Pascual, D., Hugelius, G., Canadell, J. G., Harden, J., Jackson, R. B., Georgiou, K., Jonshagen, A., Lindström, J., Ljung, K., Register, E. et al. (2026), 'Higher carbon storage in primary than secondary boreal forests in sweden', *Science* **391**(6791), 1256–1261.

Pastorello, G., Trotta, C., Canfora, E., Chu, H., Christianson, D., Cheah, Y. W., Poindexter, C., Chen, J., Elbashandy, A., Humphrey, V. et al. (2020), 'The fluxnet2015 dataset and the oneflux processing pipeline for eddy covariance data', *Scientific Data* **7**(1), 225.

Pedregosa, F., Varoquaux, G., Gramfort, A., Michel, V., Thirion, B., Grisel, O., Blondel, M., Prettenhofer, P., Weiss, R., Dubourg, V., Vanderplas, J., Passos, A., Cournapeau, D., Brucher, M., Perrot, M. and Duchesnay, E. (2011), 'Scikit-learn: Machine learning in Python', *Journal of Machine Learning Research* **12**, 2825–2830.

Peltoniemi, M., Pulkkinen, M., Aurela, M., Pumpanen, J., Kolari, P. and Mäkelä, A. (2015), 'A semi-empirical model of boreal-forest gross primary production, evapotranspiration, and soil water-calibration and sensitivity analysis'.

Pregitzer, K. S. and Euskirchen, E. S. (2004), 'Carbon cycling and storage in world forests: biome patterns related to forest age', *Global change biology* **10**(12), 2052–2077.

Preisler, Y., Grünzweig, J. M., Ahiman, O., Amer, M., Oz, I., Feng, X., Muller, J. D., Ruehr, N., Rotenberg, E., Birami, B. et al. (2023), 'Vapour pressure deficit was not a primary limiting factor for gas exchange in an irrigated, mature dryland aleppo pine forest', *Plant, Cell & Environment* **46**(12), 3775–3790.

Preisler, Y., Tatarinov, F., Grünzweig, J. M., Bert, D., Ogée, J., Wingate, L., Rotenberg, E., Rohatyn, S., Her, N., Moshe, I. et al. (2019), 'Mortality versus survival in drought-affected aleppo pine forest depends on the extent of rock cover and soil stoniness', *Functional Ecology* **33**(5), 901–912.

Reicosky, D. and Ritchie, J. (1976), 'Relative importance of soil resistance and plant resistance in root water absorption', *Soil Science Society of America Journal* **40**(2), 293–297.

Remke, M. J., Hoang, T., Kolb, T., Gehring, C., Johnson, N. C. and Bowker, M. A. (2020), 'Familiar soil conditions help pinus ponderosa seedlings cope with warming and drying climate', *Restoration Ecology* **28**, S344–S354.

Richards, L. A. (1931), 'Capillary conduction of liquids through porous mediums', *physics* **1**(5), 318–333.

Rotenberg, E. and Yakir, D. (2010), 'Contribution of semi-arid forests to the climate system', *Science* **327**(5964), 451–454.

Running, S. W. and Reid, C. P. (1980), 'Soil temperature influences on root resistance of pinus contorta seedlings', *Plant physiology* **65**(4), 635–640.

Seabold, S. and Perktold, J. (2010), Statsmodels: Econometric and statistical modeling with python, *in* '9th Python in Science Conference', SciPy.

Sendall, K. M., Reich, P. B., Zhao, C., Jihua, H., Wei, X., Stefanski, A., Rice, K., Rich, R. L. and Montgomery, R. A. (2015), 'Acclimation of photosynthetic temperature optima of temperate and boreal tree species in response to experimental forest warming', *Global change biology* **21**(3), 1342–1357.

Settele, J., Scholes, R., Betts, R. A., Bunn, S., Leadley, P., Nepstad, D., Overpeck, J. T., Angel Taboada, M., Adrian, R., Allen, C. et al. (2014), Terrestrial and inland water systems, Cambridge University Press.

Shi, H., Luo, G., Hellwich, O., Kurban, A., De Maeyer, P. and Van de Voorde, T. (2023), 'Revisiting and attributing the global controls over terrestrial ecosystem functions of climate and plant traits at fluxnet sites via causal graphical models', *Biogeosciences* **20**(13), 2727–2741.

Sinclair, V. A., Ritvanen, J., Urbancic, G., Erner, I., Batrak, Y., Moisseev, D. and Kurppa, M. (2022), 'Boundary-layer height and surface stability at hyytiälä, finland, in era5 and observations', *Atmospheric Measurement Techniques* **15**(10), 3075–3103.

Smith, M. D. (2011), 'An ecological perspective on extreme climatic events: a synthetic definition and framework to guide future research', *Journal of Ecology* **99**(3), 656–663.

Sogacheva, L., Saukkonen, L., Nilsson, E., Dal Maso, M., Schultz, D. M., De Leeuw, G. and Kulmala, M. (2008), 'New aerosol particle formation in different synoptic situations at hyytiälä, southern finland', *Tellus B: Chemical and Physical Meteorology* **60**(4), 485–494.

Sun, Z., Wang, X., Yamamoto, H., Tani, H., Zhong, G., Yin, S. and Guo, E. (2018), 'Spatial pattern of gpp variations in terrestrial ecosystems and its drivers: Climatic factors, co2 concentration and land-cover change, 1982–2015', *Ecological informatics* **46**, 156–165.

Suni, T., Rinne, J., Reissell, A., Altimir, N., Keronen, P., Rannik, Ü., Maso, M., Kulmala, M. and Vesala, T. (2003), 'Long-term measurements of surface fluxes above a scots pine forest in hyytiala, southern finland, 1996-2001', *Boreal Environment Research* **8**(4), 287–302.

Tanja, S., Berninger, F., Vesala, T., Markkanen, T., Hari, P., Mäkelä, A., Ilvesniemi, H., Hänninen, H., Nikinmaa, E., Huttula, T. et al. (2003), 'Air temperature triggers the recovery of evergreen boreal forest photosynthesis in spring', *Global change biology* **9**(10), 1410–1426.

Thom, D., Golivets, M., Edling, L., Meigs, G. W., Gourevitch, J. D., Sonter, L. J., Galford, G. L. and Keeton, W. S. (2019), 'The climate sensitivity of carbon, timber, and species richness covaries with forest age in boreal–temperate north america', *Global Change Biology* **25**(7), 2446–2458.

Van Der Sleen, P., Groenendijk, P., Vlam, M., Anten, N. P., Boom, A., Bongers, F., Pons, T. L., Terburg, G. and Zuidema, P. A. (2015), 'No growth stimulation of tropical trees by 150 years of co2 fertilization but water-use efficiency increased', *Nature geoscience* **8**(1), 24–28.

Van Genuchten, M. T. (1980), 'A closed-form equation for predicting the hydraulic conductivity of unsaturated soils', *Soil science society of America journal* **44**(5), 892–898.

Von Neumann, J. and Morgenstern, O. (2007), Theory of games and economic behavior: 60th anniversary commemorative edition, *in* 'Theory of games and economic behavior', Princeton university press.

Wang, H., Gitelson, A., Sprintsin, M., Rotenberg, E. and Yakir, D. (2020), 'Ecophysiological adjustments of a pine forest to enhance early spring activity in hot and dry climate', *Environmental Research Letters* **15**(11), 114054.

Wang, Y.-R., Buchmann, N., Hessen, D. O., Stordal, F., Erisman, J. W., Vollsnes, A. V., Andersen, T. and Dolman, H. (2022), 'Disentangling effects of natural and anthropogenic drivers on forest net ecosystem production', *Science of the Total Environment* **839**, 156326.

Wu, J., Guan, K., Hayek, M., Restrepo-Coupe, N., Wiedemann, K. T., Xu, X., Wehr, R., Christoffersen, B. O., Miao, G., Da Silva, R. et al. (2017), 'Partitioning controls on amazon forest photosynthesis between environmental and biotic factors at hourly to interannual timescales', *Global Change Biology* **23**(3), 1240–1257.

Yaseef, N. R., Yakir, D., Rotenberg, E., Schiller, G. and Cohen, S. (2010), 'Ecohydrology of a semi-arid forest: Partitioning among water balance components and its implications for predicted precipitation changes', *Ecohydrology: Ecosystems, Land and Water Process Interactions, Ecohydrogeomorphology* **3**(2), 143–154.

Zhang, Y., Xu, M., Chen, H. and Adams, J. (2009), 'Global pattern of npp to gpp ratio derived from modis data: effects of ecosystem type, geographical location and climate', *Global Ecology and Biogeography* **18**(3), 280–290.

Zhou, H., Yue, X., Wang, B., Tian, C., Lu, X., Zhu, J. and Cao, Y. (2023), 'Distinguishing the main climatic drivers to the variability of gross primary productivity at global fluxnet sites', *Environmental Research Letters* **18**(12), 124007.